1993ApJ...410..626D

THE ASTROPHYSICAL JOURNAL, 410:626–649, 1993 June 20

NEW 325 MHz OBSERVATIONS OF H II GALAXIES: THE MECHANISMS THAT SHAPE THE UNUSUAL RADIO SPECTRA

HANS-JÖRG DEEG,[1] ELIAS BRINKS,[1] NEB DURIC,[2] ULI KLEIN,[3] AND EVAN SKILLMAN[4]

Received 1992 September 11; accepted 1992 December 16

ABSTRACT

A sample of seven H II galaxies from the survey by Klein, Weiland, & Brinks (1991) was observed with the NRAO-VLA in the B array at frequencies of 325 MHz and 1489 MHz. The resulting radio continuum spectra—supplemented by values from the literature—display a wide range of spectral shapes. The spectra of two galaxies can be understood as the conventional combination of thermal and nonthermal power-law emission spectra. Four galaxies have radio spectra which show a significant flattening toward lower frequencies. The spectrum of II Zw 40 does not fit well in any category and seems to be dominated by thermal emission. The low-frequency flattening of the majority of the sample's spectra is discussed in detail invoking a variety of radio emission and absorption mechanisms and energy losses of relativistic electrons. Fits for several of these mechanisms are performed. They are (1a) synchrotron loss spectra resulting from a one-time electron injection or (1b) from a continuous electron injection which began a few Myr ago; (2) dominance of different electron loss mechanisms across the frequency range without time dependence; and (3) free-free absorption of long-wavelength radio emission by thermal electrons. The suitability of these mechanisms is discussed and model-dependent parameters like the spectral index of injected electrons, spectral index of the radio emission, the emission measure, the thermal electron density, and the age of the relativistic electrons are derived. The average spectral index of the nonthermal emission is $\alpha = 0.7 \pm 0.2$ ($S_\nu \sim \nu^{-\alpha}$) for the galaxies with flattened spectra. Only one galaxy in the sample has a very steep nonthermal spectra index of $\alpha = 1.2 \pm 0.4$. We do not find that steep nonthermal spectral indices are prevailing in H II galaxies, contradicting the expectation by Klein, Weiland, & Brinks. The presence of H II regions with thermal electron densities of ≈ 25 cm^{-3} and emission measures of a few 10^5 pc cm^{-6} is needed to establish a case for free-free absorption. For two galaxies, the approximate sizes of the H II regions required for free-free absorption can be verified from Hα images. If the spectra are interpreted as time-dependent synchrotron loss spectra, they show signs of an electron distribution generated by SNRs a few times 10^6 yr ago. Model (2) could apply only to Mkn 297. An Hα image of Mkn 297 shows starforming activity distribution over a large number of knots which are the likely result of a merger. Its radio spectrum can be interpreted as the sum of the emission from the individual knots, the ages of the starbursts in the knots not being uniform. Observations needed to discriminate between models (1) and (3) are discussed.

Subject headings: H II regions — radio continuum: galaxies — radiation mechanisms: miscellaneous

1. INTRODUCTION

In this paper we present radio continuum observations of a number of H II galaxies at 1489 MHz and 325 MHz carried out with the VLA. The purpose of these observations is to extend the observed range of radio spectra of several relatively well studied H II galaxies toward lower frequencies.

Although all of the objects we report on in this paper were taken from a sample of blue compact dwarf galaxies, we decided to refer to them as "H II galaxies" in this paper. Since their first description by Sargent & Searle (1970) as "extragalactic H II regions," many authors have studied these galaxies, using different terms to describe them, such as blue compact dwarf galaxies (BCDG), star-forming dwarf galaxies, or H II galaxies. The one characteristic shared by these galaxies is an optical spectrum resembling an H II region. Moreover, some of the galaxies in our sample would not qualify as BCDGs due to their larger linear size of $\gtrsim 10$ kpc. The main optical features of H II galaxies are high surface brightness, narrow emission lines, and blue colors from the presence of young stars produced in the starburst. They also display large, gas-rich H I envelopes, low abundances of heavy elements (or metallicities), and up to 10 times higher ratios of radio to optical luminosity than spiral galaxies. The low metallicities and the limited reservoir of gas in these galaxies imply that the currently observed blue stars must have originated in a starburst that has been either relatively recent (less than a few 10^7 yr ago) or is still ongoing. Thuan (1983) sets an upper limit for the age of the starbursts from multicolor photometry of 5×10^7 yr. Krüger et al. (1991) derive estimates for the age and duration of the starburst of the order of a few times 10^6 yr from population synthesis models. Although all galaxies which are classified as H II galaxies contain an active region of star formation, this class of objects encompasses a wide variety of underlying galaxy types. Galaxies in our sample include spiral galaxies and irregulars as well as a possible merger galaxy. This wide range of types should be kept in mind when trying to generalize results based on their common properties, e.g., of the H II regions and of the radio emission emitted by them.

The most complete work on the radio continuum spectra of

---

[1] National Radio Astronomy Observatory, PO. Box O, Socorro, NM 87801; also Institute for Astrophysics, Department of Physics and Astronomy, University of New Mexico.

[2] Institute for Astrophysics, Department of Physics and Astronomy, University of New Mexico, Albuquerque, NM 87131.

[3] Radioastronomisches Institut der Universität Bonn, Auf dem Hügel 71, D-5300 Bonn, Germany; also Max-Planck-Institut für Radioastronomie.

[4] University of Minnesota, Department of Astronomy, Minneapolis, MN 55455.

H II galaxies so far has been performed by Klein, Weiland, & Brinks (1991, hereafter KWB). Other workers reporting radio spectra of these galaxies are Sramek & Weedman (1986), Wynn-Williams & Becklin (1986), Meahara et al. (1985), Biermann et al. (1980), Klein, Wielebinski, & Thuan (1984b), Klein, Wielebinski, & Beck (1984a), Heidmann, Klein, & Wielebinski (1982), and Dressel & Condon (1978). KWB present a collection of all radio flux densities of H II galaxies for which two or more flux densities at different frequencies are available. They find that the radio continuum spectra of these galaxies are generally flatter than those of normal galaxies. In five cases—two of them have been reobserved for this paper—they have enough spectral information to separate the radio emission into thermal and nonthermal components. Steep nonthermal components with a spectral index of $\langle \alpha_{\rm nth} \rangle \leq 1.1$ (Throughout the paper we use the convention $S_\nu \sim \nu^{-\alpha}$; S is the flux density) were found, whereas the thermal components dominate above about 1 GHz. The overall shapes of the spectra were interpreted either as resulting from synchrotron losses of relativistic particles from a previous starburst in a weak (few μG) magnetic field or from particles generated in the current starburst in a strong (≤ 20 μG) magnetic field. The observations reported in this paper were initially intended as a follow-up study of KWB to differentiate between the two possibilities through 325 MHz observations which should lead to better thermal-nonthermal separations. The results we obtained went beyond these objectives. The wide variety of radio spectra necessitates a detailed assessment of several possible absorption and electron loss mechanisms, some of which allow a derivation of the age of the starburst. In § 2 the observations and sample selection are described. Section 3 describes the galaxies. In § 4 the mechanisms shaping the radio spectra are discussed, and they are treated in detail in the Appendix. Section 5 describes the fits performed on the radio spectra, and § 6 contains a discussion of the results.

2. THE OBSERVATIONS

2.1. *Sample Selection*

With the exception of II Zw 70 (Skillman & Klein 1988), no H II galaxies have been observed before at 325 MHz. Here we report on radio continuum observations of a sample of seven galaxies at 325 MHz and 1.489 GHz. Optical observations with a B filter are presented as well. Six of the galaxies were selected on the basis of a strong flux density at 5 GHz and—if known—at about 1.4 GHz from the sample in KWB. II Zw 70 was included in the sample in order to compare its 325 MHz flux with the one measured by Skillman & Klein (1988) with the Westerbork Synthesis Radio Telescope. The sample consists of relatively well studied galaxies; three of them are covered in detail by Brinks & Klein (1986).

Table 1 lists the optical positions, the radio flux densities $S_{1.489}$ and $S_{0.325}$ at 1.489 resp. 0.325 GHz which are discussed in the next section, the B band magnitudes m_B taken from the RC3 (de Vaucouleurs et al. 1991), the distance and absolute B band magnitudes M_B using $H_0 = 75$ km s^{-1} Mpc^{-1}. The optical diameter $\Theta_{\rm op}$ is taken from D_{25} in the RC3. The IR flux densities at 60 and 100 μm are taken from Wunderlich, Klein, & Wielebinski (1987). The far-infrared luminosity (FIR) is calculated using the standard formula in Helou, Soifer, & Rowan-Robinson (1985).

2.2. *VLA Observations*

Radio observations of Mkn 297, Mkn 314, Mkn 527, II Zw 40, III Zw 102, and Haro 15 were undertaken in 1990 July and of II Zw 70 in 1991 November with the NRAO–VLA.[5] At both observing dates, the VLA was in its B configuration, which has a range of baselines from 0.21 to 11.4 km. Table 2 gives the VLA observational setup. The total observing time was 7 hr, or approximately 1 hr for each object. All objects were observed at P band at a frequency of 325 MHz ($\lambda = 90$ cm) and all, except II Zw 70, at L band at 1.489 GHz ($\lambda = 20$ cm). The galaxies were observed for about 12 minutes at L band and for about 20 minutes at P band. The time on each object was distributed into three intervals ("scans") of approximately 4 minutes each at L band and 7 minutes at P band, spread over about 4 hr to achieve maximum *uv*-coverage. Exceptions were Mkn 297 for which all observations were taken on 1990 July 27 within an hour and II Zw 40, which could be observed only in the last hour of the 5 hr allocated on 1990 July 28. II Zw 70 was observed on 1991 November 15, with two scans of 16 minutes; one of them had to be discarded due to interference. The source 3C 286 was used as flux calibrator for Mkn 297 and II Zw 70 and 3C 48 as flux calibrator for the other sources. The flux densities of 3C 48 and 3C 286 were based on the Baars et al. (1977) scale. For each source an appropriate phase calibrator was observed. The L band observations were carried out in the normal continuum mode. At P band, the VLA has a strong internally generated interference at multiples of 5 and 12.5 MHz. To circumvent this interference, and to retain a large bandwidth we used spectral line mode

TABLE 1

OVERVIEW OF THE BASIC DATA

Name	Haro 15	II Zw 40	II Zw 70	Mkn 297	Mkn 314	Mkn 527	III Zw 102
α(1950)	00 46 04	05 53 05	14 48 54	16 03 01	23 00 31	23 10 41	23 18 00
δ(1950)	−12 59.45	+03 23.1	+35 47.0	+20 40.7	+16 20.0	+06 02.9	+16 57.0
$S_{0.325}$(mJy)	21.5 ± 2	38 ± 4	12.5 ± 2.5	244 ± 20	≤10	15 ± 4	68 ± 6
$S_{1.489}$(mJy)	18.5 ± 2	30.5 ± 1.5	...	104 ± 7	6.1 ± 0.5	6.5 ± 0.3	46 ± 4
m_B	13.9	15.48	14.83	13.44	14.16	14.24	12.83
Distance (Mpc)	86.0	9.2	17.4	64.3	30.3	49.1	23.9
M_B	−20.77	−14.34	−16.38	−20.60	−18.28	−19.22	−19.06
$\Theta_{\rm Op}$ (arcsec)	51	20	44	56	55	85	95
S_{60} (Jy)	1.5	7.2	0.77	7.7	1.4	4.8	9.7
S_{100} (Jy)	2.0	5.6	1.5	9.9	1.6	7.4	18.9
FIR (10^{-13} W m^{-2})	0.74	3.1	0.43	3.8	0.67	2.5	5.5

---

[5] The National Radio Astronomy Observatory is operated by Associated Universities, Inc., under cooperative agreement with the National Science Foundation.

1993ApJ...410..626D

TABLE 2

VLA OBSERVATIONAL SET-UP

Configuration	B	B
Wavelength (cm)	90	20
Observing mode	Line, 4 IF 16 channels	Continuum Full polarization
Bandwidth per channel (MHz)	0.390	...
Effective frequency/bandwidth	325/9.375 MHz	1489.9/100 MHz
Primary beam FWHM	156′	30′
Synthesized beam FWHM	22″	5″(uniform weighting)
Maximum extension of structure visible	9′	2′
Integration interval (s)	10	10
Assumed 3C 48 flux densities	$S_{325} = 43.1$ Jy	$S_{1489.9} = 15.5$ Jy
Assumed 3C 286 flux densities	$S_{325} = 26.5$ Jy	$S_{1489.9} = 14.5$ Jy

with two IF pairs, each having a bandwidth of 6.25 MHz, divided into 16 channels (Brinks 1991). The central channel for IF pair 1 was set to 320 MHz and for IF pair 2 to 330 MHz. In the calibration process, the channels with interference were removed with only a small loss in overall bandwidth. The two outer channels, which have a low gain, were removed as well. The remaining channels were averaged to create a continuum data set. Further calibration of the *L* and *P* band visibility data was performed with standard procedures in the AIPS software package. Raw maps were "cleaned" with the AIPS task "MX" which is based on the "CLEAN" algorithm by Högbom (1974), removing the side lobes of the synthesized beam with uniform weighting and restoring the "CLEAN" components with a Gaussian beam with a full width at half-maximum (FWHM) of about 22″ for the *P* band data and 5″ for the *L* band data, respectively. *P* band observations of weak sources are particularly sensitive to confusion by side lobes of stronger sources within the field of view, and extensive use of "MX" was needed for their removal. A significant increase in the signal-to-noise ratio of *P* band maps was obtained by cleaning maps from each scan individually and averaging them for the final map. For single scans, the VLA is to a good approximation a coplanar, two-dimensional array and distorting errors from the VLA's actual three-dimensionality are minimized. These errors are larger at *P* band due to the larger primary beam width and cannot be handled with current software and computing power (see, e.g., Perley & Cornwell 1991). The results of the flux density measurements are included in Table 1.

The *P* band (325 MHz) flux densities of the H II galaxies were lower than expected and special care was taken to assess the accuracy of the measurements. We evaluated the 325 MHz flux densities $S_{325\mathrm{mes}}$—corrected for primary beam attenuation—of background sources measured from our maps by identifying them with sources whose flux S_{408} at 408 MHz is listed in the "Ohio Masterlist of Radio Sources" (Dixon 1970, last update 1981). Cataloged 408 MHz sources could be found around four of the seven galaxies observed and are given in Table 3. They are from the Parkes catalog (Day et al. 1966), denoted as PKS, and from the MC3 catalog (Sutton et al. 1974). MC3 flux densities were preferred to PKS densities. The 408 MHz flux densities S_{408} were extrapolated to 325 MHz flux densities $S_{325\mathrm{ex}}$ using a power law with spectral index α. For PKS sources α was taken from Day et al. (1966), who obtained it from 408 MHz, 1410 MHz, and 2650 MHz flux densities. For some MC3 sources, α was calculated using 178

TABLE 3

SOURCES AROUND THE GALAXIES USED IN THE VERIFICATION OF OUR 325 MHZ FLUX DENSITIES

Name[a]	Alternative Name[b]	S_{408}[c]	α[d]	Note[e]	$S_{325\mathrm{ex}}$[f]	$S_{325\mathrm{mes}}$[g]	Agree[h]
Near II Zw 40:							
PKS 0558+02	...	2.6 ± 1	0.60 ± 0.50	1	2.98 ± 1.20	2.62 ± 0.26	Yes
Near Mkn 314:							
MC3 2254+167	PKS, 4C 16.80	4.5 ± 0.37	0.80 ± 0.30	1	5.40 ± 0.58	6.50 ± 0.65	Yes
MC3 2257+163	...	0.39 ± 0.09	0.85 ± 0.30	3	0.47 ± 0.11	0.18 ± 0.02	No
MC3 2258+166	4C 16.81	1.29 ± 0.15	0.90 ± 0.28	2	1.58 ± 0.21	1.80 ± 0.18	Yes
MC3 2304+156	4C 15.77	1.09 ± 0.14	0.85 ± 0.29	2	1.32 ± 0.19	1.22 ± 0.12	Yes
Near Mkn 527:							
PKS 2310+05	...	9.1 ± 1.3	0.70 ± 0.10	1	10.67 ± 1.54	12.10 ± 1.21	Yes
Near III Zw 102:							
MC3 2314+160	...	0.93 ± 0.15	0.85 ± 0.30	3	1.13 ± 0.20	0.95 ± 0.10	Yes
MC3 2315+155	PKS, 4C 15.78	1.51 ± 0.12	0.70 ± 0.50	1	1.77 ± 0.25	2.25 ± 0.23	Yes

[a] Name of the source in the PKS resp. MC3 survey.

[b] PKS means that source is also in PKS MHz survey, 4C name from 179 MHz survey given if available.

[c] S_{408}: Flux density from MC3 survey or PKS survey.

[d] Spectral index α between 325 and 408 MHz.

[e] Notes to α: (1) α was taken from PKS catalog; (2) α calculated between S_{408} and flux density at 179 MHz from 4C survey; (3) α was taken as 0.85 ± 0.30.

[f] 325 MHz flux extrapolated from S_{408} and α.

[g] 325 MHz flux densities measured in this work.

[h] Indicates if $S_{325\mathrm{ex}}$ and $S_{325\mathrm{mes}}$ overlap with their error bars.

MHz flux densities from the 4C survey, if available. For the remaining MC3 sources, a spectral index of $\alpha = 0.85 \pm 0.30$ was taken, which is expected for extragalactic, synchrotron radiation–dominated objects. The extrapolated flux densities $S_{325\mathrm{ex}}$ agree with our measured flux density $S_{325\mathrm{mes}}$ within their error bars in seven out of eight cases. For these seven cases the ratio of extrapolated to measured flux, $S_{325\mathrm{ex}}/S_{325\mathrm{mes}}$, is 1.05 ± 0.17.

None of the background sources in our 1.489 GHz maps could be identified in the list by Dixon due to the much smaller field of view at 1.489 GHz. However, a comparison of these weaker, uncataloged background sources at 1.489 GHz with their counterparts in the 325 MHz maps showed that the average spectral index was around 0.75. This lends additional support to our flux densities at 90 cm.

2.3. *Optical Imaging*

Optical CCD images were obtained at the Capilla Peak Observatory[6] 0.6 m telescope for five of the seven galaxies in 1990 October and of Mkn 297 in 1991 May. The images were taken in *B* band with exposure times of 30 minutes per filter. Standard procedures for image processing were performed using IRAF. In this paper, only a presentation of overlays between 1.489 GHz radio maps and the *B* broad-band images is given. II Zw 70 has not been imaged by us yet, and we refer to the B band image given by Barbieri, Bonoli, & Rafanelli (1979). Imaging of the galaxies in the Hα line was attempted at the NOAO Kitt Peak[7] 0.9 m Telescope in 1992 January. That observing run was mostly clouded out and only images of II Zw 40, II Zw 70, and Mkn 297 were obtained under non-photometric conditions. A full account of the optical observations will the subject of a forthcoming paper.

3. DISCUSSION OF THE INDIVIDUAL GALAXIES

In Figures 1*a*–1*f* we present the *L* band (1.489 GHz) radio continuum maps of six of the sample galaxies, with a resolution of about 5″. II Zw 70 has not been observed at *L* band and is not shown. The *P* band maps are not shown since they do not exhibit any resolved structure with a beam size of about 22″. The *L* band contour maps have been overlaid onto gray-scale *B* band CCD images. The absolute positioning of the CCD images has been obtained by using stars which appear on the CCD frames and measuring their position on POSS prints with the measuring engine. The final positioning is precise to $\leq 0\rlap{.}''5$. The relative positioning between radio and optical images should be accurate to about $0\rlap{.}''5$ as well. The precision of the radio positions depends on the positional precision of the phase calibrator sources, which were taken from the VLA calibrator list and are known to within $0\rlap{.}''1$.

Figure 1*a* shows the 1.489 GHz emission of Haro 15 (= Mkn 960 = MCG −02-03-019) closely following the blue light distribution. A local radio flux density maximum of 2.0 ± 0.4 mJy is centered on the optical knot at $0^{\mathrm{h}}46^{\mathrm{m}}5\rlap{.}^{\mathrm{s}}28$, $-12°59'24\rlap{.}''4$, about 4 kpc southeast of the center. Another local radio maximum with a flux density of ≤ 0.5 mJy coincides with a detached region of optical light emission at $0^{\mathrm{h}}46^{\mathrm{m}}5\rlap{.}^{\mathrm{s}}6$, $-12°59'08''$ about 9 kpc northeast of the center.

II Zw 40 (= UGCA 116 = CGPG 0553.1 + 0324) is shown in Figure 1*b*. Comparison with the map of KWB confirms the reality of the southern extension seen here, which may be associated with the optical plumes also visible in our CCD image and previously reported by Baldwin, Spinrad, & Terlevich (1982). The maximum optical emission coincides with our radio peak to within 1″.

Mkn 297 (= NGC 6052 = UGC 10182 = CGCG 1603.0 + 2041 = MCG +04-38-022 = VV 086 = Arp 209 = CGCG 137-032) (Fig. 1*c*). Yin & Heeschen (1991) consider Mkn 297 to consist of two interacting galaxies and identify two radio supernovae (RSNs) within Mkn 297. One of the RSN, Mkn 297A, is responsible for Mkn 297's previously reported (Heeschen, Heidmann, & Yin 1983) variable flux density. Mkn 297A is at the position of maximum flux density. The 1.5 GHz peak flux density of 15 ± 2 mJy per beam area in our map is significantly higher than Yin & Heeschen's last observation of Mkn 297A with 4.7 ± 0.1 mJy in 1990 July, but they include only baselines longer than 2.5×10^4 wavelengths to suppress the extended emission. Using previous observations of Mkn 297A, they derive a date for the SN explosion of 1979 July. A second possible RSN, Mkn 297B, is detected by them, not wholly unexpected in the light of Mkn 297's estimated supernova rate of 0.3–0.5 yr^{-1} (Klein et al. 1986). Yin & Heeschen's detection of Mkn 297B is not confirmed by Lonsdale, Lonsdale, & Smith (1992), who observed Mkn 297 in 1991 August with the VLA and report on a VLBI detection of Mkn 297A. They obtain an upper limit to its size of 2 mas and a lower limit on the brightness temperature of 6×10^8 K at 1.5 GHz. They consider the question if Mkn 297A is an RSN or an AGN as yet unresolved. If Mkn 297A is indeed an RSN, it would be the most powerful one known. The radio luminosity of Mkn 297A at 1.5 GHz is about 5% of Mkn 297's total luminosity, which is mostly from an extended envelope which seems to follow the northern and southern optical knots.

The map of Mkn 314 (= NGC 7468 = UGC 12329 = CGCG 453-0.52 = CGCG 2300.5 + 1620) (Fig. 1*d*) shows that there is a significant displacement between the radio and the optical emission, the latter being shifted by almost 4″ (≈0.5 kpc) westward. This radio position is somewhat less accurate, only to about 2″, since the position of the closest phase calibrator turned out to be inaccurate and a more distant phase calibrator was used as a position reference. The offset radio peak is suggestive of RSN as in Mkn 297, and it is planned to reobserve Mkn 314 in the near future. The radio emission is slightly extended towards the north and southwest.

The peak of the radio emission of Mkn 527 (= CGCG 2310.6 + 0603 = MCG +01-59-012 = NGC 7518 = UGC 12422 = CGCG 406-020) (Fig. 1*e*) falls some 3″ (≈0.8 Kpc) northeast of the bright optical nucleus. The underlying CCD image gives the overall impression of Mkn 527 being a small barred spiral galaxy.

III Zw 102 (= NGC 7625 = UGC 12529 = CGCG 2318.0 + 1657 = MCG +03-59-038 = VV 280 = Arp 212 = CGCG 454-043 = CGPG 2318.0 + 1637) (Fig. 1*f*) is surrounded by extensive dust with some strong dust lanes. The radio emission does not reflect the extent of the dust envelope. Moreover, it seems that the radio emission decreases in the vicinity of the shell type structure to the northeast of the center.

The galaxy II Zw 70 (= MrK 0829 = UGC 09560 = CGCG 1448.9 + 3547 = MCG +06-33-002 = VV 324b = CGCG

---

[6] Capilla Peak Observatory is operated by the Institute for Astrophysics of the University of New Mexico.

[7] Kitt Peak National Observatory, a division of the National Optical Astronomy Observatories, is operated by Association of Universities for Research in Astronomy, Inc., under a cooperative agreement with the National Science Foundation.

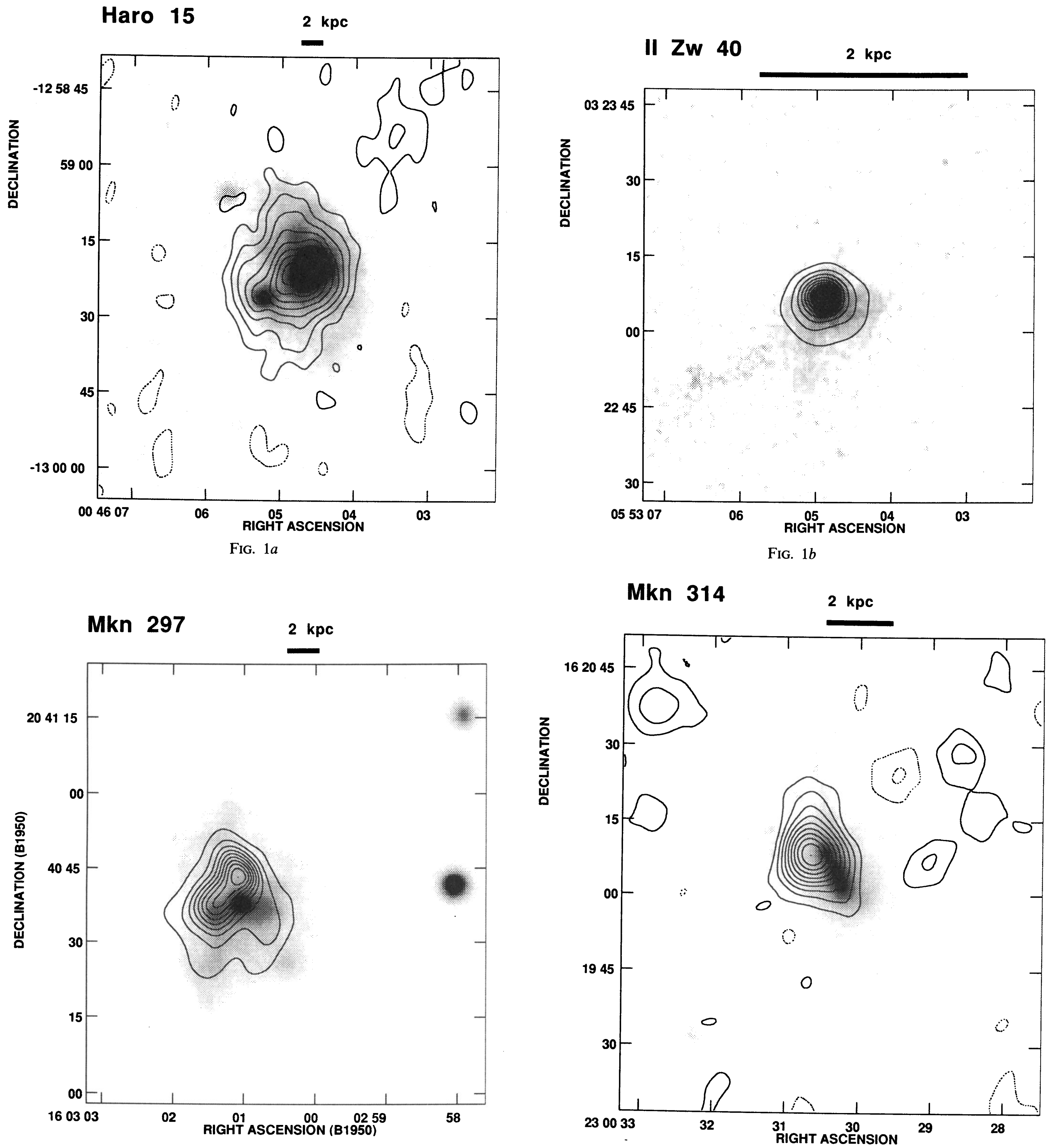

FIG. 1*a*

FIG. 1*b*

FIG. 1*c*

FIG. 1*d*

FIG. 1.—Contour maps of the six galaxies observed at $\nu = 1.489$ GHz overlaid on optical *B*-band CCD images. The contour lines are at 10% intervals of the peak flux density per beam area. The peak flux densities are Haro 15: 2.7 mJy, II Zw 40: 12.1 mJy, Mkn 297: 15.1 mJy, Mkn 314: 3.4 mJy, Mkn 527: 3.8 mJy, III Zw 102: 4.4 mJy. The beam FWHM is 5″. The bar on the top of each figure corresponds to a linear distance of 2 kpc.

1993ApJ...410..626D

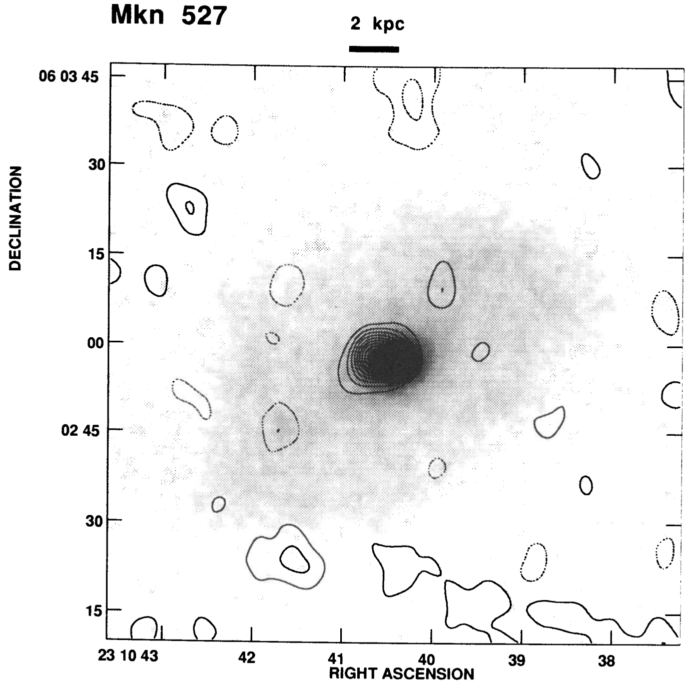

FIG. 1*e*

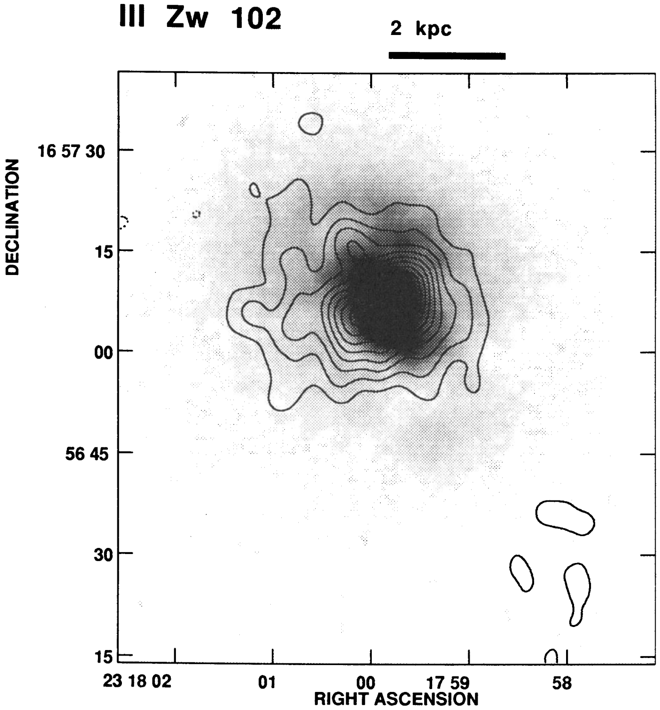

FIG. 1*f*

193-004 = CGCG 1448.9+3547 = CG 0560) was not observed at *B* band or 1.489 GHz. It is described by Barbieri et al. (1979) as having a bright nucleus with two extensions.

In Figures 2*a*–2*g* the radio flux densities for all galaxies are plotted, at higher frequencies supplemented by values from the literature as collected by KWB. The flux densities used for the plots are listed in Table 4. The fits to the data shown in Figure 2 are discussed in §§ 5 and 6. Figure 3 shows the absolute, distance corrected radio power of all seven galaxies.

TABLE 4

RADIO FLUX DENSITIES KNOWN TO DATE FOR THE SEVEN GALAXIES OF THIS INVESTIGATION

Galaxy	ν [GHz]	Sν [mJy]	Reference
Haro 15	0.325	21.5±2	This paper
	1.489	18.5±2	"
	4.750	13±2	Klein, Wielebinski and Beck (1984)
	10.500	6±2	Klein et al. (1991)
	10.700	6.6±0.5	"
II ZW 40	0.325	38±4	This paper
	1.415	30±0.5	Jaffe et al. (1978)
	1.465	29.9±0.7	Klein et al. (1991)
	1.465	28.2±1.1	Deeg & Brinks (May 91)
	1.489	30.5±1.5	This paper
	4.750	22±3	Klein, Wielebinski and Beck (1984)
	4.885	21.0±1.9	Klein et al. (1991)
	5.000	22±4	Jaffe et al. (1978)
	10.700	21±2	Klein et al. (1991)
	10.550	19.2±1.8	"
	24.500	18±4	Klein, Wielebinski and Thuan(1984)
II ZW 70	0.325	12.5±3.0	This paper
	0.327	11.2±2.0	Skillman and Klein (1988)
	0.610	6.5±0.8	"
	1.415	5.0±0.6	Balkowski et al. (1978)
	1.465	4.3±1.0	Wynn-Williams and Becklin (1986)
	4.750	3.4±1.0	Klein, Wielebinski and Thuan (1984)
	4.750	2.5±1.1	Skillman and Klein (1988)
	4.885	3.0±1.0	Wynn-Williams and Becklin (1986)
	10.700	2.7±0.2	Klein, Wielebinski and Thuan (1984)
	10.700	4.4±1.0	Klein et al. (1991)
	10.700	4.1±2.0	Skillman and Klein (1988)
Mkn 297	0.325	244±20	This paper
	1.489	104±7	This paper
	4.750	42±3	Klein, Wielebinski and Beck (1984)
	4.750	42.4±1.1	Klein et al. (1991)
	4.750	40.8±1.4	"
	4.885	31±6	Biermann et al. (1980)
	10.500	21.2±2.0	Klein et al. (1991)
	10.700	26±2	Heidmann et al. (1982)
	10.700	22±5	Klein et al. (1991)
	10.700	24±4	Meahara et al. (1985)
	22.800	11±1	Heidmann et al. (1982)
	24.500	14±3	Klein et al. (1991)
	32.000	< 12	"
Mkn 314	0.325	≤10	This paper
	1.465	6.7±0.9	Klein et al. (1991)
	1.489	6.1±0.5	This paper
	4.885	3.6±0.4	Klein et al. (1991)
Mkn 527	0.325	15±4	This paper
*	1.465	10.3±1.0	Klein et al. (1991)
	1.489	6.5±0.3	This paper
	4.885	4.3±0.5	Klein et al. (1991)
III ZW 102	0.325	68±6	This paper
	1.465	50.7±2.0	Klein et al. (1991)
	1.489	46±4	This paper
	2.380	37.0±4.0	Dressel and Condon (1978)
	4.750	27.0±4.0	Klein, Wielebinski and Beck (1984); corrected in Klein et al. (1991)
	4.750	24.0±1.0	Klein et al. (1991)
	4.750	26.0±3.0	"
	4.885	24.5±2.1	"
	10.500	14.2±2.0	"
	10.700	16.7±1.0	"
*	24.500	24.0±5.0	"

* Flux densities probably overestimated due to confusion with nearby source.

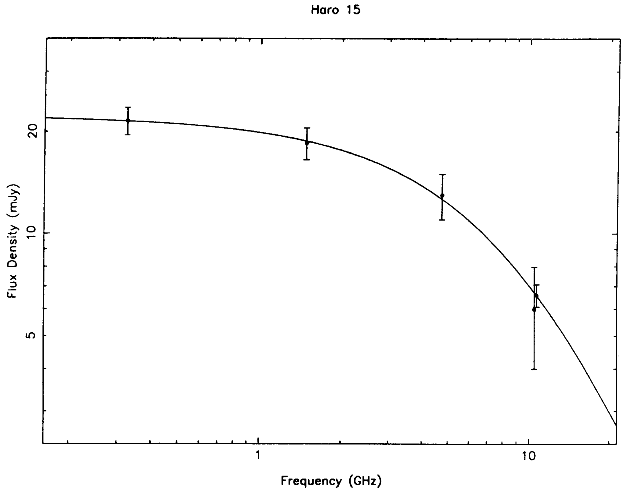

FIG. 2*a*

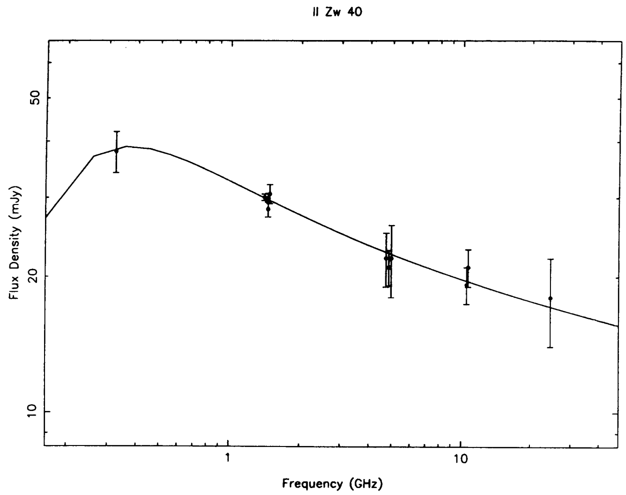

FIG. 2*b*

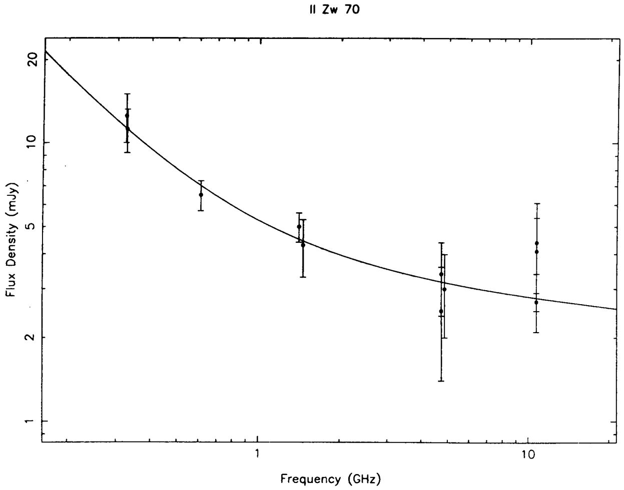

FIG. 2*c*

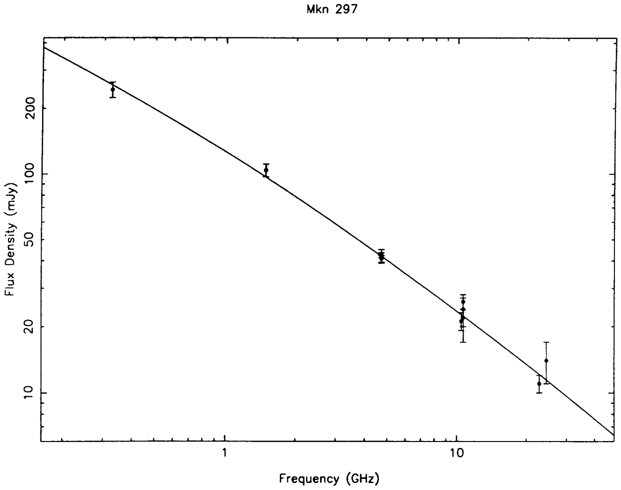

FIG. 2*d*

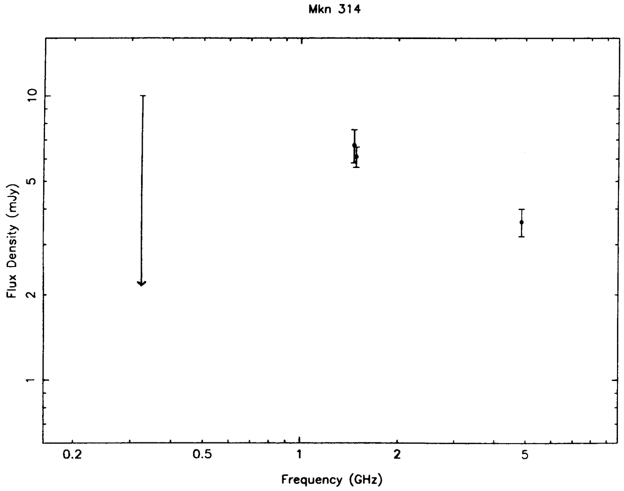

FIG. 2*e*

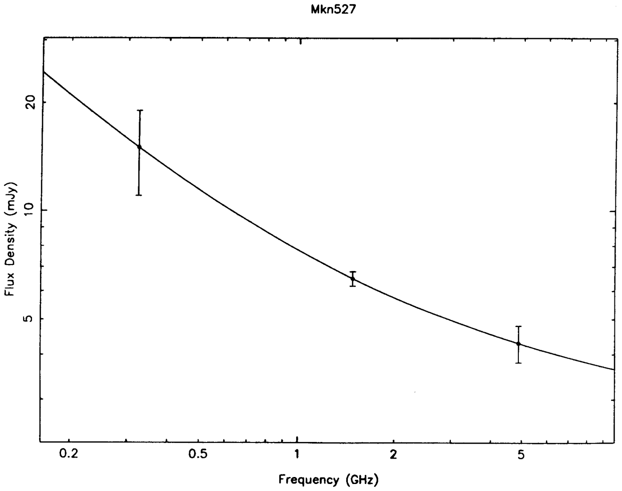

FIG. 2*f*

FIG. 2.—Plots of the flux density data of Haro 15 as a function of frequency. The values quoted for the higher frequencies were taken from KWB. The fit shown is of function I_1 (one-time injection of CR electrons at time t' ago). (*b*) As Fig. 2*a* for II Zw 40. The fit is of function I_6 (free-free absorption and emission) using a diameter Θ of the absorbing region of 9″. (*c*) As Fig. 2*a* for II Zw 70. The fit is of function I_7 (thermal-nonthermal separation). (*d*) As Fig. 2*a* for Mkn 297. The fit is of function I_3 (dominance of different loss mechanisms). (*e*) As Fig. 2*a* for Mkn 314. No fits. (*f*) As Fig. 2*a* for Mkn 527. The fit is of function I_7 (thermal-nonthermal separation). (*g*) As Fig. 2*a* for II Zw 102. The solid line is a fit of function I_2 (injection of CR electrons since time t'). The dashed line is a fit of function I_6 (free-free absorption and emission) using a diameter Θ of the absorbing region of 3″.

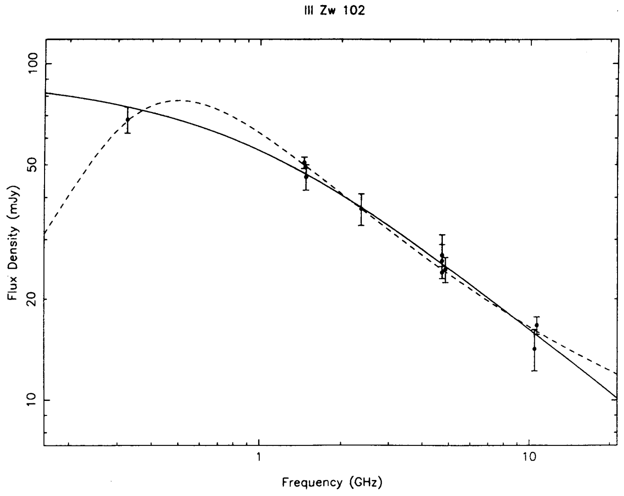

FIG. 2*g*

4. MECHANISMS SHAPING THE RADIO SPECTRA IN H II GALAXIES

There are two radio emission mechanisms which we need to consider: nonthermal or synchrotron emission, which is bremsstrahlung emitted from gyrating *relativistic* electrons in a magnetic field, which results in radio emission described by a power law $S_\nu \sim \nu^{-\alpha}$, where a typical value for extragalactic sources is $\alpha \approx 0.75$. The other mechanism is thermal or free-free emission which is collisional bremsstrahlung emitted by thermal electrons in an ionized gas, which results in flat radio spectra approximated by $S_\nu \sim \nu^{-0.1}$. Formulae for these emission mechanisms are given in Appendix A. The radiation emitted by warm interstellar dust is only significant at submillimeter wavelengths and can be neglected at centimeter wavelengths.

KWB made an attempt to separate thermal and nonthermal components in a few H II galaxies. The resulting nonthermal spectral indices were steep, typically $\alpha_{\rm nth} \geq 1.1$, where $S_\nu \sim \nu^{-\alpha}$. The addition of the 325 MHz values from our measurements shows a flattening of the spectra in four out of seven cases, contrary to KWB's expectation that the 325 MHz frequency measurements would yield values with reflect steep nonthermal spectra (Figs. 2 and 3). The steepest low-frequency spectra found in our work have $\alpha_{\rm nth} \approx 0.9$, (see Table 5), but more generally they are $\alpha_{\rm nth} \approx 0.5$, indicating a flattening rather than a steepening toward lower frequencies.

To explain the flattening we have to invoke a variety of physical processes beyond radio emission mechanisms. They are briefly discussed in this section and in detail in the Appendix. An assessment of the relative influence of these mechanisms is given in § 6, which is based on the fits to the radio spectra described in § 5. If no units are noted in the formulae, the appropriate CGS unit should be taken.

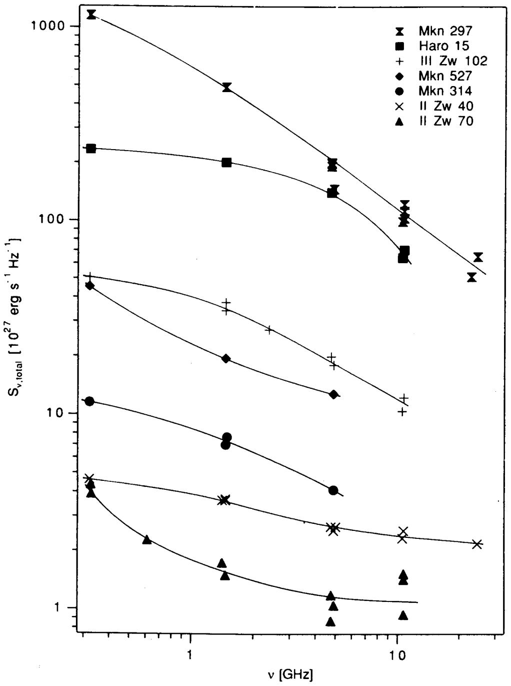

FIG. 3.—Absolute, distance-corrected radio fluxes for all seven galaxies

Several of the mechanisms depend on the galaxy's magnetic field strength which is obtained by assuming equipartition between the energy of the magnetic field and the energy of the relativistic particles. Here we use (Pacholczyk 1970)

$$B = [6\pi(1 + k)c_{12} V^{-1} L_{\rm syn}]^{2/7} , \tag{1}$$

where k is the ratio of the energies stored in relativistic protons versus electrons, c_{12} is a weakly varying function of the spectral index α, V is the emission volume, and $L_{\rm syn}$ is the synchrotron luminosity. The proton-to-electron ratio k has been derived from direct measurements in interplanetary space, where it was found to be $k \approx 40 \pm 8$ for particles with 1 GeV (Webber 1991, and references therein). As the spectral index of electrons and protons is about the same, the ratio of energies is equal to the number ratio of protons to electrons. We adopt the value $k = 40$ but are aware of its uncertainty, particularly in the light of recent results indicating a lower proton-to-electron ratio toward the anticenter of our galaxy (Pohl & Schlick-

TABLE 5

VALUES USED IN EQUIPARTITION CALCULATIONS

Name	Haro 15	II Zw 40	II Zw 70	Mkn 297	Mkn 314	Mkn 527	III Zw 102
S_{ν_0} (mJy)	13	5	2.0	94	6.4	6.5	25
ν_0 (GHz)	4.75	1.489	1.0	1.489	1.489	1.489	4.75
$\alpha_{\rm nth}$	0.6	0.68	1.2	0.80	0.50	0.9	0.70
$\Theta_{1.4}$ (arcsec)	16.5	8.5	$<25^{\rm a}$	12.8	11.4	7.1	17.5
$\Theta_{1.4}$ (kpc)	6.8	0.38	2.1	4.0	1.7	1.7	2.0
$L_{\rm syn}$ (10^{38} ergs cm^{-2})	45	0.27	0.077	66	1.7	2.5	6.3
B (μG)	15	33	11	33	19	30	28

[a] Upper limit estimated from 325 MHz map. No 1.4 GHz map available.

eiser 1991). To obtain V we use the volume of a spherical emission region with an approximate diameter $\Theta_{1.4}$ obrained from our 1.489 GHz maps. To calculate $L_{\rm syn}$ we used

$$L_{\rm syn} = 4\pi d^2 \int_{\nu_1}^{\nu_2} S_{\nu 0}\left(\frac{\nu}{\nu_0}\right)^{-\alpha} d\nu \ , \qquad (2)$$

where d is the distance of the galaxy in cm, $S_{\nu 0}$ is the observed flux density at a reference frequency ν_0, α the synschrotron spectral index, and $\nu_1 = 10^7$ Hz, the lower frequency cutoff and $\nu_2 = 10^{11}$ Hz, the upper cutoff. Table 5 lists the values used, and the results of the equipartition calculations. In this table $S_{\nu 0}$ is the estimated nonthermal flux density at the frequency ν_0; α is an approximate nonthermal spectral index taken from the fits; $\Theta_{1.4}$ is the diameter of a circle with the same area as the radio emitting region at a 50% contour level, taken from 1.489 GHz maps. $L_{\rm syn}$ is the absolute synchrotron luminosity, calculated for a lower frequency cutoff at 0.01 GHz and an upper one of 100 GHz using the spectral index α. B is the magnetic field strength derived from equipartition calculations.

Before treating any mechanism which shapes the radio spectra, a comment on the possibility of the radio spectra just merely reflecting the injected cosmic-ray (CR) electron spectra is merited. A synchrotron radiation–dominated spectrum with $S \sim \nu^{-\alpha}$ is related to the CR electron spectrum $N(E) \sim E^{-\gamma}$ by $\alpha = (\gamma - 1)/2$, reflecting the electron energy spectrum. The dominant frequency of the synchrotron emission depends on the energy of the relativistic electrons by equation (A1) (in the Appendix). It might be possible that the synchrotron spectrum is produced by young CR electrons and the observed radio spectra reflects the energy spectrum of the electrons. This should lead to speculations about CR acceleration mechanisms which produce low-energy CRs with a very flat injection spectrum. We are not aware of such an acceleration mechanism.

Exact solutions for the synchrotron radio spectrum emitted from a power-law electron distribution $N(E) \sim E^{-\gamma}$ with an upper cutoff at $E_{\rm H}$ [i.e., $N(E) = 0$ for $E > E_{\rm H}$) are given by Kardashev (1964) and are discussed in the textbook by Pacholczyk (1970). Tables for normalized radio emission in such a case are given by Packholczyk (1977). The energy results in a very steep fall-off in synchrotron radiation for $\nu(E > E_{\rm H})$. Such a steep fall-off is generally not seen in radio spectra and would be difficult to observe due to the low synchrotron flux densities at high frequencies and contamination by thermal emission. Therefore, in the further discussion, we will ignore energy cutoffs in the *injected* electron spectra and assume that they are power laws given by $N(E) \sim E^{-\gamma_0}$ without any cutoffs, where γ_0 is the spectral index of the injected electron distribution.

The electromagnetic radiation emitted from electrons injected with a power-law energy distribution can be modified by a variety of mechanisms. The mechanisms can be divided into those that influence the energy distribution of the relativistic electrons (which cause synchrotron emission) and those which influence the electromagnetic radiation directly. A list of possible mechanisms is given below, the mechanisms are treated in more detail in Appendices B and C.

Processes shaping the energy distribution of the relativistic electrons include the following:

1. Synchrotron and inverse Compton losses (CR aging) of relativistic electrons.
2. Electron energy losses through free-free interactions (inelastic scattering).
3. Convective electron energy losses.
4. Coulomb (elastic scattering) and ionization losses.

Processes affecting the electromagnetic radiation directly include the following:

1. Razin-Tsytovich effect (increase in the refractive index of the medium).
2. Synchrotron self-absorption.
3. Free-free absorption of electromagnetic radiation.

The radiation spectra from electrons undergoing synchrotron losses with a time-dependent power-law injection spectrum are given for two simple cases in Appendix B. Equations (B10)–(B14) give the spectrum for the case in which an initial distribution of relativistic electrons at a time t' ago is not replenished anytime latter. Such a spectrum has a break given by $\Delta\alpha = (\gamma_0 + 5)/6$, with γ_0 being the spectral index of the injected electron distribution. If inverse Compton losses are dominating, or the pitch angle of the electrons with respect to the magnetic field gets constantly isotropized, then the spectrum has a very steep fall-off at higher frequencies. If synchrotron losses are dominant and a continuous injection of electrons was "turned on" at a time t' ago, the break in the spectrum is $\Delta\alpha = 0.5$, see equations (B19)–(B23). In all cases, there is a steepening of the radio spectra at a characteristic frequency $\tilde{\nu}_T$, given by equation (B11) for synchrotron losses only and by equation (B24) for synchrotron and inverse Compton losses. The energy loss rate from inverse Compton losses (eq. [B6]) depends on the energy density of the electromagnetic radiation $\mu_{\rm rad}$, which can be calculated from the far infrared flux (FIR; see Table 1) density by: $\mu_{\rm rad} = 4\pi I/c$, where the intensity I is $I = 1/\pi$ FIR/$\Delta\Omega$; $\Delta\Omega$ is the solid angle of the emitting region. $\Delta\Omega$ was determined from the optical diameter ($\Theta_{\rm op}$ in Table 1) and should present a lower limit of the FIR-emitting volume. Values for $\mu_{\rm rad}$ range from 0.15 to 10 eV cm^{-3}. Inverse Compton losses are of the same magnitude as synchrotron losses in II Zw 40 only and are much less in the other galaxies.

Synchrotron and inverse Compton losses steepen an electron spectrum in the energy range where they are dominant. Among the remaining electron energy loss mechanisms, inelastic scattering and convective electron energy losses leave the spectral index unchanged whereas Coulomb and ionization losses flatten the spectrum. Spectral breaks can occur, if different energy losses dominate across the electron energy range. Generally, the loss mechanisms which steepen the spectra are dominant at the high-frequency end, whereas the losses which lead to a flattening dominate at low frequencies. An overview of the energy losses caused by ionization losses, free-free losses, synchrotron, and inverse Compton losses at electron energies responsible for radio emission is given in Figure 4. The values for the thermal electron density, the magnetic field and $\mu_{\rm rad}$ are representative for the environment in our sample galaxies. It should be noted that for an electron energy range of 10^8–10^{10} eV, which corresponds to a frequency range of a few MHz to several GHz in a magnetic field of a few μG, free-free losses can be the dominant loss mechanism if the density of H II is on the order of a few atoms per cm^{-3}. The high star formation rate in H II galaxies would make such a high H II density plausible. Independent measures of the H II density through the determination of emission measures from Hα imagery are desirable, as well as a better determination of the fraction of synchrotron radiation to thermal bremsstrahlung.

Let us next turn our attention to effects which shape the electromagnetic radiation spectrum directly. The Razin-

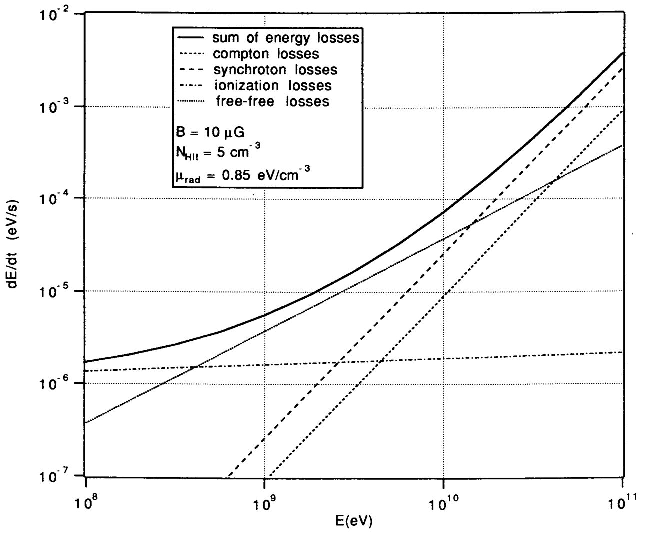

FIG. 4.—Plot of the energy loss of relativistic electrons due to a variety of loss mechanisms. The magnetic field used in the calculation is 10 μG, the thermal gas density is 5 cm^{-3}, and the electromagnetic radiation density is $\mu_{\rm rad} = 0.85$ eV cm^{-3}.

Tsytovich effect (eq. [C1]) will not be of significance at frequencies above 20 MHz, using typical values for the electron density of 10 cm^{-3} and the magnetic field strength of 10^{-5} G. Using equation (C3), typical source diameters for H II galaxies, the 325 MHz flux density values, and typical spectral indices (e.g., 0.7) it can be easily shown that synchrotron self-absorption can be excluded as well, as it will be only significant at frequencies of the order of a few MHz. A possible exception might be Mkn 297, where a flux density of ≈ 5 mJy is reported in a region with a size of $\approx 10^{-5}$ arcsec^2 in the source Mkn 297A using VLBI measurements (Lonsdale et al. 1992). Here, synchrotron self-absorption could occur at frequencies of approximately 100 MHz. This leaves free-free absorption of electromagnetic radiation by an unbound thermal gas for further discussion. Free-free *absorption of radiation* should not be confused with the free-free *losses of relativistic electrons* mentioned in the previous paragraph. "Free-free absorption" is usually referred to as "bremsstrahlung self-absorption," but in our case the electromagnetic radiation absorbed is mostly synchrotron radiation and we cannot speak of a "self-absorption" process. Free-free absorption can potentially make H II regions opaque for the lowest frequencies in our observed spectral. The optical depth τ can easily be calculated if the absorbing medium is between the emitting medium and the observer (eq. [C5]) and if the absorbing and the emitting medium fills the same space (eq. [C7]). The opacity is very strongly frequency dependent with $\tau \sim \nu^{-2.1}$. Estimates of the opacity can be used to derive the emission measure EM $= \int n_{\rm H\,II^2}\, dl$, where $n_{\rm H\,II}$ is the H II density, which in turn can be used to derive lower limits for the thermal emission. This procedure is outlined in more detail in the next section.

5. FITTING OF SPECTRAL CURVES TO THE OBSERVED DATA

Using those mechanisms discussed in § 4 which may contribute to the spectral shape of our observed spectra, we attempted several different types of fits to the data. These are discussed in sequence. The application of these fits to the individual galaxies will be discussed in § 6. The fits were performed by minimization of the χ^2 errors between fit and data using the Levenberg-Marquardt Method as given by Press et al. (1988). Errors for the fitted parameters were obtained from the resulting covariance matrix. The significance of the fits was calculated using the data normalization procedure given by Pohl, Schlickeiser, & Hummel (1991). The significance does not make any statement about the reliability of the parameters obtained in a fit. It is merely a measure for the goodness of the fit, to be used to compare fits of different models to the same data set. For radio spectra where there are several differing flux density values at the same frequency—as for example with Mkn 297—it is principally not possible to obtain a fit with a small χ^2 error respectively a very high significance.

The fits attempted for the galaxies with a convex spectrum are discussed in order.

1. Spectra resulting from relativistic electrons undergoing synchrotron losses with a time-dependent source function. To these processes we want to refer as "synchrotron aging." For the case of a one-time electron injection at a time t' ago, which is identical to a ceasing of the injection t' ago, this involves a fit based on equation (B12)

$$I_1(\nu) = k \cdot \tilde{B}\left(\frac{\nu}{\tilde{\nu}_T}, \gamma_0\right) \tag{3}$$

to the data, where the fitted parameters are the proportionality constant k, the break frequency $\tilde{\nu}_T$, and the spectral index γ_0 of the injected electron distribution. Using equation (B11), the time since injection t' can be obtained from $\tilde{\nu}_T$. Similarly,

$$I_2(\nu) = k \cdot \tilde{C}\left(\frac{\nu}{\tilde{\nu}_T}, \gamma_0\right) \tag{4}$$

was fitted to test the scenario when electron injection began a time t' ago and remains at a constant level up to the present; see equation (B20). No fits to inverse Compton loss–dominated spectra were performed, since inverse Compton losses are about two orders of magnitude lower than synchrotron losses for all galaxies with convex spectra. However, estimates for parameters derived from the break frequency $\tilde{\nu}_T$ using equation (B24) should be correct for synchrotron and inverse Compton loss–dominated spectra.

2. A radiation spectrum with a change in its spectral index $\Delta\alpha = 0.5$ results from the dominance of different loss mechanisms across the frequency range. Grouping the loss mechanisms by their dependence on E, the energy loss rate $\varphi(E) = dE/dt$ is given by

$$\varphi(E) = E^2(\xi_s + \xi_{\rm com}) + E(\eta_{\rm ff} + \eta_{\rm con}) , \tag{5}$$

where ξ_s and $\xi_{\rm com}$ are the energy-independent loss rates for synchrotron and inverse Compton losses respectively (see eqs. [B5] and [B6]). For free-free losses and convective losses the loss rates are $\eta_{\rm ff}$ and $\eta_{\rm con}$, see equations (B25), (B26), and (B27). Ionization and Coulomb losses were not considered in the fits, as they do not dominate the electron losses in the frequency range considered. With the sums of the loss rates: $\xi = \xi_s + \xi_{\rm com}$ and $\eta = \eta_{\rm ff} + \eta_{\rm con}$, the energy loss rate can be written as

$$\varphi(E) = E(E\xi + \eta) .$$

Using equation (B2), with the usual electron source function $q(E) \sim E^{-\gamma_0}$, the electron distribution in a time-independent case is then given by

$$N(E) \sim \frac{E^{-\gamma_0}}{E\xi + \eta} . \tag{6}$$

1993ApJ...410..626D

$N(E)$ has a change in spectral index of $\Delta\gamma = 1$ around $E_b = \eta/\xi$. Since that spectral break occurs very gradually across the frequency range (see Fig. 4), it is valid to use equation (A3) and approximate the synchrotron emission spectrum by

$$I_3(\nu) = c \cdot \frac{\nu^{-\alpha+1/2}}{1 + (\nu/\nu_b)^{1/2}} \tag{7}$$

which has a spectral break of $\frac{1}{2}$; c is an arbitrary factor; $\alpha = \gamma_0/2$ and gives the spectral index of the steeper part of the spectrum which is dominated by synchrotron or inverse Compton losses (see eq. [B7]). With the frequency-energy relations (A4) and (A5), ν_b is given by

$$\frac{\nu}{\nu_b} = \frac{E^2\xi^2}{\eta^2}\,. \tag{8}$$

Formula (7) was fitted to the data with the free parameters c, α, and ν_b. It turned out that the "spectral break" in equation (7) is very smooth and can only fit well the spectrum of Mkn 297.

3. Free-free absorption at low frequencies.

We initially fitted functions for the case in which an absorbing medium lies between the observer and emitter:

$$I_4(\nu) = c\nu^{-\alpha} \exp\left(-\tau_1 \nu^{-2.1}\right)\,. \tag{9}$$

I_4 is based on equation (C5), where τ_1 is the frequency independent term of the optical depth (see eq. [C4]):

$$\tau_1 = 8.3 \cdot 10^{-2} T_e^{-1.35}\left(\frac{\mathrm{EM}}{\mathrm{pc\ cm^{-6}}}\right)\,. \tag{10}$$

The case of an absorbing and emitting medium occupying the same volume is fitted by

$$I_5(\nu) = c\nu^{-\alpha+2.1}\left[1 - \exp\left(-\tau_1 \nu^{-2.1}\right)\right] \tag{11}$$

which is based on equation (C7). The fitted parameters were c, α, and τ_1. It turned out that the fits resulting from I_4 and I_5 are nearly indistinguishable and the further discussion is based on I_5, where the emission and absorbing media are in the same volume. The determination of τ_1 from the fits allows the calculation of the emission measure EM, assuming an H II temperature of 10^4 K. Using EM, the absolute thermal flux density S_{th} at 5 GHz can be obtained from (Mezger & Henderson 1967):

$$\left[\frac{S_{\mathrm{th}}(5\ \mathrm{GHz})}{\mathrm{mJy}}\right] = 0.143 T_e^{-0.35}\left(\frac{\Theta^2}{\mathrm{arcmin}}\right)\left(\frac{\mathrm{EM}}{\mathrm{pc\ cm^{-6}}}\right)\,, \tag{12}$$

where Θ is the diameter of the emission region. S_{th} depends on the frequency with $S_{\mathrm{th}} \sim \nu^{-0.1}$ (see Appendix A, § A 2). $S_{5\mathrm{th}}$ in terms of τ_1 is

$$\left(\frac{S_{\mathrm{th}}(\nu)}{\mathrm{mJy}}\right) = 2.04 T_e \tau_1\left(\frac{\Theta^2}{\mathrm{arcmin}}\right)\left(\frac{\nu}{\mathrm{GHz}}\right)^{-0.1} \tag{13}$$

Whereas I_5 assumes only synchrotron radiation being emitted, fitting a conbination of I_5 and equation (13) includes thermal emission as well. This is achieved by modifying the emission coefficient in equation (C6) to account for both emission mechanisms. The fits will give upper limits to the thermal flux density S_{th} which in turn set upper limits to the emission measures. The function fitted was

$$I_6(\nu) = \left(c \cdot \nu^{-\alpha+2.1} + 2.04 T_e \Theta^2 \nu^2\right)\left[1 - \exp\left(-\tau_1 \nu^{-2.1}\right)\right]\,, \tag{14}$$

where T_e and Θ were fixed input parameters and c, α, and τ_1 were fitted. The diameter Θ of the thermal region has to be smaller than the diameter $\Theta_{1.4}$ of the continuum emission. Fits of I_4, I_5, and I_6 allow the derivation of the emission measure EM from τ_1 assuming a value of T_e which we took as 10^4 K. For fits resulting from I_6, the thermal gas density $n_{\mathrm{H\,II}}$ can be obtained from EM if a gas column length $L_{\mathrm{H\,II}}$ is assumed, then $n_{\mathrm{H\,II}} = (\mathrm{EH}/L_{\mathrm{H\,II}})^{1/2}$. $L_{\mathrm{H\,II}}$ was taken from the angular diameter Θ and the galaxy's distance, assuming that $L_{\mathrm{H\,II}}$ is the same as the emission region's absolute diameter. Fits of I_6 for small diameters Θ yield the same parameters as fits of I_5.

4. Last, we detail with the fits to concave spectra. To Mkn 527 and II Zw 70, both displaying a concave spectrum, we fitted spectra resulting from a superposition of thermal and a nonthermal emission. The flat thermal radiation spectrum is dominant at $\nu \gtrsim 5$ GHz (eq. [A8]), whereas the nonthermal synchrotron radiation has a steeper power-law spectrum and dominates at lower frequencies (e.g., Duric, Bourneuf, & Gregory 1988); see equations (A1)–(A3). This is the same fit as was attempted by KWB for some galaxies in our sample but without the low-frequency data points. The spectra are approximated by

$$I_7(\nu) = S_{\mathrm{th}}\left(\frac{\nu}{\mathrm{GHz}}\right)^{-0.1} + S_{\mathrm{nth}}\left(\frac{\nu}{\mathrm{GHz}}\right)^{-\alpha_{\mathrm{nth}}}\,, \tag{15}$$

where S_{th} and S_{nth} are the thermal and nonthermal flux densities at a nominal frequency of 1 GHz and α_{nth} is the nonthermal spectral index.

Tables 6A–6F give the results of the fits for all galaxies except for Mkn 314 which does not have enough reliable data points. The tables list the mechanisms fitted, the significance of the fits, and the parameters obtained from the fits. Fits to I_1 and I_2 result in a value for the injected electron spectral index γ_0. We choose to quote a value for γ_0 as a result for all other fits as well under the assumption that the nonthermal emission is dominated by synchrotron losses (see eq. [B7]); i.e., $\gamma_0 = 2\alpha$. Values for the spectral index α for fits I_3 and I_5 result from the approximation of an underlying power-law radio spectrum $S \sim \nu^{-\alpha}$ at the steepest part of the spectrum and disregard thermal emission. Thermal emission is considered in the fits I_6 and I_7, where α denotes the *nonthermal* spectral index. The value f_{th} is the percentage of the thermal emission on the total radio emission at 1 GHz. Values which are in brackets have errors which are of the order of the size of the value or larger than the value itself. No errors are given for f_{th}, the emission measure EM, the H II density $n_{\mathrm{H\,II}}$, and the synchrotron age t'. These values depend only indirectly on the results of the fits and are based on reasonable assumptions of T_e to derive EM, and on T_e and $L_{\mathrm{H\,II}}$ to derive $n_{\mathrm{H\,II}}$, whereas t' depends on the (equiparation) magnetic field strength as $B^{3/2}$; hence the derived values should be interpreted as fair estimates for their order of magnitude. Figure 2*a*–2*g* show one or more of the fits mentioned in Tables 6A–6F overlaid on the data.

6. DISCUSSION OF THE RESULTS

We have presented radio continuum observations of a small sample of H II galaxies at 325 MHz and 1.489 GHz. The unusual radio spectra are analyzed for a variety of mechanisms. Only one galaxy in the sample, II Zw 70, had been observed previously at comparatively low frequencies by Skillman & Klein (1988) who expected its radio spectrum to be representative for this class of galaxies. This turned out not to

TABLE 6A

RESULTS OF FITS ON HARO 15

mechanism		sig.	parameters from fits				
				γ_o		t' [10^6 yrs]	
I_1: injection was t' ago		96%		1.25 -1.52		1.2	
I_2: injection since t'		68%		(1.28-2.1)		3	
			α	γ_o		EM[10^5pc cm^{-6}]	
I_5: free-free absorption		71%	0.55±0.07	1.1±0.15		5.1	
I_6: free-free absorption & emission			α	γ_o	f_{th}[%]	EM[10^5pc cm^{-6}]	n_{HII}
	d=1"	70%	0.59±0.19	1.18±0.4	4.1	5.4	34
	d=2"	62%	(0.73)	(1.46)	18	5.8	25
	d=3"	40%	(0.63)	(1.26)	24	2.7	14

TABLE 6B

RESULTS OF FITS ON II ZW 40

mechanism		sig.	parameters from fits				
			α				
simple power law		97%	0.21±0.03				
I_6: free-free absorption & emission			α	γ_o	f_{th}[%]	EM[10^5pc cm^{-6}]	n_{HII}
	d = 3"	99.0%	1.94±0.15	3.88±0.3	56	15	101
	d = 4"	98.9%	1.61±0.18	3.22±0.4	63	8.2	65
	d = 5"	98.7%	1.33±0.21	2.66±0.4	66	5.1	46
	d = 7"	98.3%	0.92±0.30	1.84±0.6	67	2.5	27
	d = 9"	97.7%	0.68±0.34	1.36±0.7	65	1.5	18
	d =11"	97.0%	0.53±0.42	1.06±0.8	62	0.88	13
	d = 15"	95.8%	(0.40)	(0.80)	55	0.42	7.6

TABLE 6C

RESULTS OF FITS ON II ZW 70

mechanism	sig.	parameters from fits		
		α		
simple power law	89%	0.34±0.04		
I_7: thermal-nonthermal separation		α	γ_o	f_{th}[%]
	98.0%	1.22±0.4	2.44±0.8	65

TABLE 6D

RESULTS OF FITS ON MKN 297

mechanism		sig.	parameters from fits				
				γ_o		t' [10^6 yrs]	
I_1: injection was t' ago		78%		2.24±0.08		0.6	
I_2: injection since t'		84%		1.66±0.14		7	
I_3: synchrotron vs.			α	γ_o		ν_b[GHz]	
free-free losses		80%	(0.92)	(1.84)		(2.25)	
			α	γ_o		EM[10^5pc cm^{-6}]	
I_5: free-free absorption		84%	0.79±0.05	1.58±0.1		2.3	
I_6: free-free absorption & emission			α	γ_o	f_{th}[%]	EM[10^5pc cm^{-6}]	n_{HII}
	d = 1"	84%	0.80±0.05	1.60±0.10	0.3	2.3	27
	d = 2"	81%	0.81±0.07	1.62±0.15	1.2	2.3	20
	d = 3"	71%	0.86±0.12	1.72±0.25	2.9	2.5	17
	d = 4"	50%	0.84±0.16	1.68±0.32	3.6	1.7	12

TABLE 6E

Results of Fits on Mkn 527

mechanism	sig.	parameters from fits		
I_7: thermal-nonthermal		α	γ_o	f_{th}[%]
separation	100%	0.89±0.48	1.78±1.0	51

TABLE 6F

Results of Fits on III Zw 102

mechanism	sig.	parameters from fits				
			γ_o		t' [10^6 yrs]	
I_1: injection was t' ago	93%		1.68±0.1		2.0	
I_2: injection since t'	98.9%		1.32±0.2		10	
		α	γ_o		EM[10^5pc cm^{-6}]	
I_5: free-free absorption	99.7%	0.59±0.03	1.18±0.06		3.9	
I_6: free-free absorption						
& emission		α	γ_o	f_{th}[%]	EM[10^5pc cm^{-6}]	n_{HII}
d = 2.5"	99.6%	0.70±0.07	1.40±0.15	8.5	4.8	40
d = 3"	99.6%	0.82±0.16	1.64±0.32	14	5.8	40
d = 4"	97.6%	0.84±0.27	1.68±0.55	20	4.2	30
d = 6"	79%	0.66±0.29	1.32±0.60	19	1.5	15

be the case. The spectra of the galaxies observed show a great diversity. The most prominent feature is the flattening of the spectral index towards lower frequencies for the majority of galaxies in the sample. This flattening or spectral turnover is much more pronounced than in nonthermal spiral galaxies (Israel & Mahoney 1990). Based on the morphology of their radio spectra (see Fig. 3), we will split our sample into three groups:

1. *Concave spectrum.*—II Zw 70 and Mkn 527 can readily be described by the superposition of thermal and nonthermal emission power laws. The fraction of thermal emission at 1 GHz, $f_{\rm th}$ (see Tables 6c and 6e), is rather higher in both galaxies, with 65% for II Zw 70 and 51% for Mkn 527.
2. *Convex spectrum.*—Haro 15, Mkn 314, and III Zw 102 show a pronounced low-frequency flattening in their radio spectra. For these galaxies on flux densities at $\nu \gtrsim 10$ GHz are known. Their spectra are steep at the high-frequency end. An upper limit to the thermal fraction is $f_{\rm th} \approx 20\%$ at 1 GHz. The 325 MHz flux of Mkn 314 is an upper limit only and makes its spectrum unsuitable for a detailed analysis. Mkn 297 has a comparatively minor change in its spectral index. Its spectrum is entirely dominated by nonthermal emission. The thermal emission has an upper limit of $f_{\rm th} \approx 3\%$ at 1 GHz.
3. *Flat spectrum.*—The radio spectrum of II Zw 40 is very flat with a spectral index of $\alpha = 0.21 \pm 0.03$ and appears dominated by thermal emission with $f_{\rm th} \gtrsim 55\%$. This makes a determination of its nonthermal spectral index very uncertain.

To analyze this inhomogeneous set of radio spectra, a wide range of mechanisms influencing the shapes of radio spectra has been introduced in § 4 and the Appendices. These mechanisms fall into two categories: energy loss mechanisms of the relativistic, synchrotron radiation–emitting electrons and mechanisms which influence the electromagnetic radiation directly. Particular attention was given to the way these mechanisms influence the radio spectra. Electron energy loss mechanisms are grouped together by the power index of their dependency on the electron energy. Among other causes for spectral flattening, the presence of energy cutoffs in the relativistic electron distribution was ruled out, as well as synchrotron self absorption and the Razin-Tsytovich effect. Only free-free absorption deserves closer scrutiny. The galaxies with a convex spectrum were fitted to several of the possible mechanisms. All of the fits yielded either values for the spectral index of the nonthermal radiation α or for the spectral index of the injected electron distribution γ_0, and one or more parameters specific to the fitted mechanism. For the two galaxies with a "conventional" concave spectrum, separations into thermal and nonthermal emission were obtained. Values derived indirectly from the fits, such as emission measures, gas densities, ages of relativistic electrons, etc., should be understood as representing estimates for their order of magnitude—being useful to discuss the plausibility of one or the other model. These words of caution are warranted since errors are accumulated from the parameters obtained in the fits, from parameters which have been derived outside of the fits (for example the equipartition magnetic field strength), and from the fact that all parameters are integrated properties over entire galaxies. Our equipartition calculations result in relatively high magnetic fields of 10–30 μG. The mechanisms discussed in the following paragraphs are all inherently coupled to the specific conditions present in H II galaxies.

6.1. *Thermal-Nonthermal Separation: The Galaxies with Concave Spectra*

The two galaxies with a concave spectrum, Mkn 527 and II Zw 70, can readily be described by the superposition of thermal and nonthermal power-law spectra; they have steep nonthermal spectral indices. Our reobservation of II Zw 70 at 325 MHz agrees well with the flux densities given by Skillman & Klein (1988). Its nonthermal spectral index is $\alpha = 1.22 \pm 0.4$; for Mkn 527 it is $\alpha = 0.9$. In both galaxies, the nonthermal radiation is probably caused by electrons whose entire observed energy spectrum has been steepened by synchrotron losses. In this case the relation between radio spectral index α, and electron injection spectrum is $\gamma_0 = 2\alpha$, the values for γ_0 obtained that way are included in Tables 6c and 6e. Any spectral break from electron aging processes would have to be below the lowest frequency observed, i.e., at $\nu_T \lesssim 325$ MHz. Using equation (B11), this leads to minimum ages of the relativistic electrons of 5.1×10^7 yr for II Zw 70 and 1.2×10^7 yr for Mkn 527. Another possible interpretation would be that the nonthermal radiation in those two galaxies is from very young electrons whose energy spectrum has *not* yet been steepened by synchrotron losses. In that case, an upper limit of the age of the sources could be given from $\nu_T \gtrsim 1$ GHz. A spectral break in the nonthermal radiation at higher frequencies is unlikely to be observable in these sources, since higher frequency radiation is dominated by the strong thermal emission. Then, upper limits for the electron ages are 2.8×10^7 yr for II Zw 70 and 6.6×10^6 yr for Mkn 527. However, the injection spectral index is given in this case by $\gamma_0 = 2\alpha + 1$. This leads to unacceptably steep injection spectral indices of $\gamma_0 = 3.4$ for II Zw 70 and $\gamma_0 = 2.8$ for Mkn 527.

6.2. *Convex Radio Spectra*

In this section the results for Haro 15, Mkn 297, and III Zw 102 and are dealt with, discussing in turn the different mechanisms which play a role in shaping the observed radio spectra.

6.2.1. *Time-dependent Relativistic Electron Injection*

The first possibility investigated is that of electron spectra resulting from time-dependent injection spectra. This mechanism has been applied to the irregular dwarf NGC 1569 by Israel & de Bruyn (1988) who interpret NGC 1569 as a post-starburst galaxy, where the injection of CR electrons sharply declined about 5×10^6 yr ago. Radio spectra, with a one-time electron injection at a time t' ago, have a change in the spectral index from α for $\nu < \nu_T$ to $(4/3\alpha + 1)$ for $\nu > \nu_T$, where ν_T is the frequency of the break. This scenario is used in fitting function I_1. Spectra where the injection *began* t' ago (fitting function I_2), have a spectral break of $\Delta\alpha = 0.5$, where the break occurs over a much narrower frequency range than in the model involving dynamical halos as discussed in the next paragraph. It should be noted that for time-dependent spectra, the spectral index for electrons with $\nu < \nu_T$, which are not yet affected by synchrotron and inverse Compton losses, is $\alpha = (\gamma_0 - 1)/2$. This is the same as for free-free losses, as follows from equation (B4) with $\kappa = 1$. Hence, a possible dominance of free-free losses or adiabatic deceleration at $\nu \lesssim \nu_T$ does not change the interpretation of time-dependent spectra. In our model fits, electron aging by synchrotron and inverse Compton losses leads to ages t' of typically a few 10^6 yr. We did not make assumptions about any thermal emission; all three galaxies have $f_{\text{th}} \lesssim 20\%$. A subtraction of thermal emission from the data as performed by Israel & de Bruyn (1988) would lead to a steeper spectrum mainly at high frequencies but would not change the results of the fits with respect to the turnover frequency. Such a reevaluation of the fraction of the synchrotron emission (which is assumed to be 100% in the current calculations) lowers the values of the magnetic field obtained by equipartition calculations and in turn increases the estimates of the synchrotron aging time t'. Under the current assumptions, the magnetic fields obtained are typically 25 μG and values for t' are of the order of a few 10^6 yr. Under these circumstances, the CR electrons would have to be from a starburst which is very recent or still ongoing. This is in agreement with Israel & de Bruyn's (1988) analysis of NGC 1569. The diffusion confinement time for electrons with the critical energy E_T, which dominate the radio emission at the spectral break frequency ν_T, with E_T given by equations (A4), (A5), and (B24), is a few 10^7 yr which indicates that electrons at the spectral break are not significantly depleted by diffusion. The galaxies Mkn 297 and III Zw 102 could be fitted to both of the time-dependent electron injection scenarios with about the same, good statistical significances. Haro 15 permits a good fit only for fitting function I_1, the scenario of an electron injection t' ago. Fits of I_1 lead to ages t' of 0.6–2 Myr for the three galaxies. The scenario where electron injection began t' ago (fitting function I_2) leads to flatter electron spectral indices γ_0, to lower break frequencies ν_T, and larger ages t' of 7 Myr of Mkn 297 and 10 Myr for III Zw 102.

6.2.2. *Different Electron Energy Losses at Different Frequencies*

Spectral breaks of $\Delta\alpha = 0.5$ or $\Delta\alpha = 1.0$ result, if electron loss mechanisms with different energy dependencies dominate at different frequencies. The most detailed work on the influence of electron energy losses on radio spectra has been done by Lerche & Schlickeiser (1982) and by Pohl & Schlickeiser (1990). Their work shows a spectral break in the integrated radio emission of $\Delta\alpha = 0.5$ if adiabatic deceleration losses in a dynamical halo are present. Since energy-independent loss mechanisms—like ionization losses—were ruled out in § 4, we consider only the dominance of free-free losses and adiabatic cooling losses over synchrotron and inverse Compton losses, which gives a spectral break of $\Delta\alpha = 0.5$. Pohl et al. (1991) made a statistical analysis of a sample of normal spiral galaxies where they confirmed such a spectral break in a majority of cases, resulting from a dynamical halo. Hummel (1991) in his reinterpretation of the spectra of late spiral galaxies from Israel & Mahoney (1990) argues for a spectral break due to a dynamical halo as well. The change of $\Delta\alpha = 0.5$ occurs only very gradually across the frequency range, which cautions against fits based on two straight power laws. Although several galaxies (Haro 15, Mkn 297, III Zw 102) could be interpreted as having a break of $\Delta\alpha = 0.5$, only Mkn 297's spectral index changes smoothly enough to result in fits with a significance comparable to that of other mechanisms.

6.2.3. *Free-Free Absorption*

Shaping the radio continuum spectra of galaxies by free-free absorption was proposed by Israel & Mahoney (1990). Their 57.5 MHz flux density detections for a sample of mostly late-type spirals were lower than expected from extrapolations from higher frequency flux densities. Their conclusion is that free-free absorption as well as nonthermal emission occurs in a clumpy medium with small filling factors. The density in the clumps is of the order of 1 cm^{-3} and electron temperatures are $500 \lesssim T_e \lesssim 1000$ K. They discount free-free absorption by a smoothly distributed ionized gas component; such a component would require very low electron temperatures of $T_e \approx 50$ K. The authors claim a weak dependence of the low frequency absorption on the galaxies' tilt as is expected from an absorption mechanism. These findings are disputed by Hummel (1991), who finds the absorption-versus-tilt dependency to be statistically insignificant and concludes that propagation losses of relativistic electrons (see previous section) are at least equally plausible. In an analysis of the radio spectrum of M33, which has a turnover at 500–900 MHz, Israel, Mahoney, & Howarth (1992) support the conclusions of Israel & Mahoney (1990).

In our fits, we initially used two scenarios: free-free absorption by a medium between the radio-emitting region and the observer (fit I_4), and free-free absorption in the same volume in which the radio-emission occurs (fit I_5). The two fitting functions, I_4 and I_5, produced nearly indistinguishable fits. Direct parameters obtained are the radiation spectral index α, and the optical depth by free-free absorption. Assuming an electron temperature T_e, the emission measure EM can be derived. The formulae for free-free absorbed spectra imply a steep decline of $S \sim \nu^{-2.1}$ at low frequencies; they assume just a single emission measure across the absorbing region. A distribution of emission measures across the absorbing region will lead to a smearing of the frequencies at which free-free absorption becomes relevant.

TABLE 7

Results from Fits of Free-Free Absorption at Selected Absorption/Emission Sizes and Filling Factors of 1

Name	H II size	H II size (kpc)	EM (pc cm^{-6})	$M_{\rm H\,II}$ ($M_\odot$)
Haro 15	1″	0.46	5.4e5	8.3e7
II Zw 40	5	0.24	5.1e5	1.6e7
Mkn 297	2	0.61	2.4e5	1.1e8
III Zw 102	2.5	0.36	4.8e5	2.7e7

A more complete fit (I_6) evaluates the emission measure EM in two ways: EM determines the optical depth by free-free absorption (as before in fit I_5) *and* the amount of thermal emission. Using a volume filling factor $f = 1$, fits of I_6 yield upper limits on the angular size of the thermal absorbing/emitting region (see Tables 6A–6G). This limit is quite well defined, as the thermal emission depends on the square of the region's size; see equation (13). If exceeded, the significances of the fits gets rapidly lower, e.g., maximum angular sizes obtained are about 3″ for Mkn 297, corresponding to a linear size of 900 pc, and 4″ for III Zw 102 (Tables 6D and 6F), corresponding to 600 pc. As smaller thermal regions do generate less thermal emission, $f_{\rm th}$ is lower, and there is less free-free absorption; the emission measures obtained for them are lower, but the gas densities required are higher than in bigger thermal regions. The spectral indices α obtained from good fits are in the range of 0.6–0.9, leading to injected electron indices γ_0 of 1.2–1.8. These values for γ_0 agree well with those obtained from the fit I_2 for synchrotron aging. Fits to free-free absorption were performed for II Zw 40 as well. This galaxy seems dominated by thermal emission and is treated in more detail in a section later in this paper. The sizes of the free-free absorbing regions can be principle be verified from Hα images. At present, Hα images are available for Mkn 297 and II Zw 40, neither galaxy showing a pronounced spectral flattening. The diameter of the most prominent H II regions in these galaxies are 2″.5 and 4″, respectively, which does not disagree with the diameters required to fit I_6. Figures 5*a* and 5*b* show Hα images of Mkn 297 and II Zw 40, respectively, taken with the NOAO Kitt Peak 0.9 m telescope.

However, there are problems in the interpretation of free-free absorption in the radio spectra while assuming a filling factor "f" of unity: the emission measures needed for the observed optical depths are of the order of a few 10^5 pc cm^{-6}, resulting in large, yet not unreasonably high H II masses of a few 10^7 $M_\odot$. Table 7 gives emission measures and H II masses resulting from the best fits of I_6 with $f = 1$. H II regions with EM $\approx 10^5$ pc cm^{-6} are not uncommon (see, e.g., the table of H II regions in Lang 1980), but they are all small with diameters of the order of 5–50 pc and masses of typically a few 100 to less than a few 1000 $M_\odot$. H II galaxies, on the other hand,

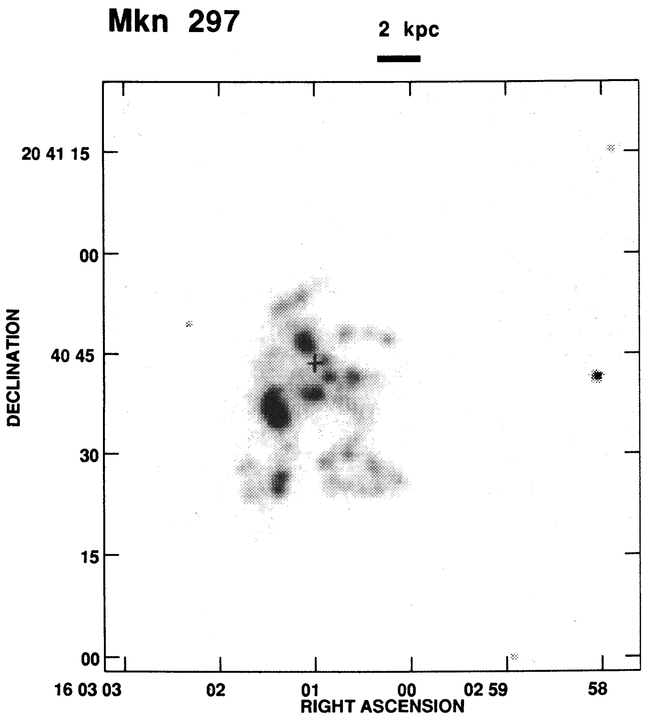

FIG. 5*a*

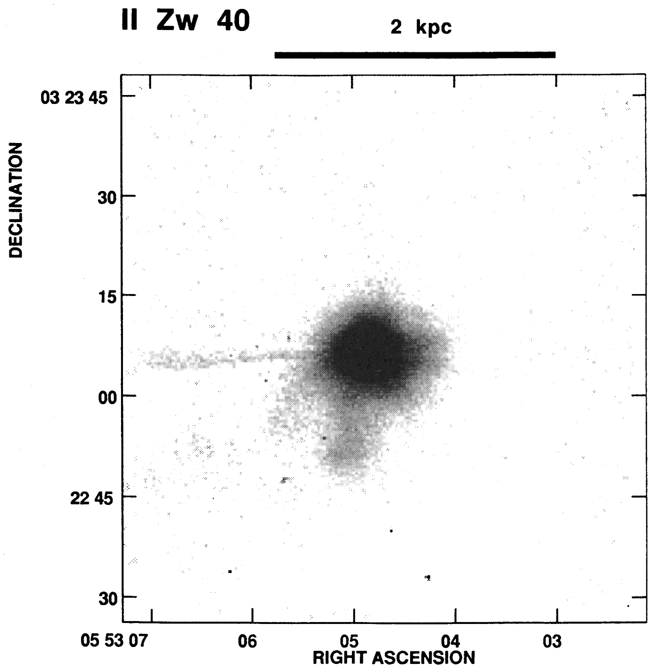

FIG. 5*b*

FIG. 5.—(*a*) CCD image of Mkn 297 in the Hα + [N II] line. The cross indicates the position of Mkn 297A. (*b*) CCD image of II Zw 40 in the Hα + [N II] line. The extension to the left is an artefact from the CCD chip.

commonly have very large H II regions; see, e.g., the Hα image of II Zw 40 (Fig. 5b), indicating active star formation. The emission measure at a given optical depth and the electron temperature are related by EM $\sim T_e^{1.35}$. H II galaxies have generally very low metallicities which lower cooling rates in H II regions. Hence it is not unlikely that T_e exceeds 10^4 K and might be as high as 2×10^4 K, requiring even higher emission measures for significant free-free absorption. The presence of a cooler ionized gas component, as proposed by Israel & Mahoney (1990) for spiral galaxies, would relax the constraints on the size of the absorbing regions considerably. In a cooler gas, smaller emission measures would suffice to generate the same optical depths as in a hotter gas. Our results for free-free absorption in a 10^4 K gas require emission measures of a few 10^5 pc cm^{-6} and electron densities of typically $n_e > 30$ cm^{-3} (see fits to U_5 and I_6 in Tables 6A–6F). At gas temperatures of 1000 K, the emission measures would be of the order of 10^4 pc cm^{-6}. Densities of cool ionized gas of 2 cm^{-3} at a filling factor of 1 could achieve these emission measures on scale sizes only about twice as large than the higher density medium at 10^4 K, assuming that this cooler component lies well outside the region of active star formation. The scale size would of course increase with f_c^{-1}, if the cool component is in clumps and f_c is the line-of-sight filling factor of the clumps which was assumed to be $f_c \approx 0.1$ by Israel & Mahoney. However, we prefer the idea that free-free absorption takes place in a high-density, 10^4 K medium, i.e., within the star formation region itself. We point out that the sizes of the H II regions needed and the emission measures at these temperatures are not unrealistic for the H II galaxies under study.

The emission measures derived from the fits are actually *lower* limits since we assume synchrotron radiation and free-free absorption occurring in the same area. Only synchrotron emission that is generated in, or is going through an area with free-free absorption on its way to the observer gets absorbed. If the free-free–absorbing area fills only part of the synchrotron-emitting area, even higher emission measures are needed. If we define a ratio "A" between the nonthermal emitting area and the thermal absorbing area, then even in the idealized case with free-free–absorbing regions of optical depth $\tau = \infty$ and no foreground synchrotron emission, it has to be $A \gtrsim 0.3$ for Mkn 297, Mkn 314, and Haro 15 and $A \gtrsim 0.45$ for II Zw 102. It can be shown that all nonthermal emission is likely to be emitted within the thermal H II regions in these galaxies, thus sustaining high surface filling factors. We estimate the distance which relativistic electrons can diffuse from their origin before losing their energy. The diffusion distance depends on the diffusion speed, which is taken to be the Alfvén speed, and on the time scale in which relativistic electrons decelerate from very high energies to energies of about 2 GeV, which corresponds to synchrotron emission of about 300 MHz. Under these assumptions, relativistic electrons will move less than 100 pc from their origin—presumably the site of an O-star supernova remnant (SNR) in an H II region—before they lose enough energy to become irrelevant for synchrotron emission The Hα image of Mkn 297 (Fig. 5a) shows several larger H II knots with diameters of about 500 pc. II Zw 40 (Fig. 5b) shows one central Hα region with a diameter of about 200 pc. At least in these two galaxies it might be the case that a large fraction of the nonthermal emission is emitted within thermal, free-free–absorbing H II regions. However, given the uncertainty of the filling factor, it is questionable, if the emission measures in these H II regions are high enough for significant free-free absorption at 325 MHz.

6.2.4. *Mkn 297*

Mkn 297 fits well to all the previously mentioned mechanisms and has the weakest, yet significant bend in its spectrum. The influence of the one, or possibly two radio supernovae (RSNs) in Mkn 297 is discussed here. If we use the integrated flux density values of Mkn 297 from 13 to 1.5 GHz and extrapolate them with a straight power-law toward 325 MHz, the 325 MHz flux density $S_{325\mathrm{ex}}$ is 340 ± 20 mJy, whereas the measured 325 MHz flux density $S_{325\mathrm{mes}}$ is 244 ± 20 mJy, which leaves a flux deficiency of $\gtrsim 55$ mJy. The integrated flux density of the RSN Mkn 297A is about 5% of the total flux density both at 1.5 and 5 GHz, using the most recent flux densities from Yin & Heeschen (1991) and Lonsdale et al. (1992). The expected flux density of Mkn 297A at 325 MHz can be extrapolated using the results from the fits of Chevalier's model (Chevalier 1984) to Mkn 297A's light curves at 1.5 GHz and 5 GHz given by Yin & Heeschen. The radio emission in the early stages of an RSN is dominated by free-free absorption. Chevalier's model predicts an optical depth by free-free absorption for the RSN's 325 MHz emission of $\tau \approx 0.62$ at the time of our observations, and a flux density of about 9 mJy. However, the term which gives τ in Yin & Heeschen's fit depends on only one data point in the rising slope of the RSN and might be quite unreliable. An upper limit for the RSN's flux density at 325 MHz of $\lesssim 20$ mJy is obtained by assuming no free-free absorption and by extrapolation from the 1.5 and 5 GHz values; a lower limit would assume a very high optical depth and no significant flux from Mkn 297A at 325 MHz. This means, that even if Mkn 297A is completely obscured at 325 MHz, it cannot contribute more than 20 mJy to Mkn 297's integrated flux deficiency of $\gtrsim 55$ mJy. The other possible RSN, Mkn 297B, which has been observed only by Yin & Heeschen, had a peak flux of about 55% of Mkn 297A in 1990 July, which might contribute another 10 mJy to the integrated 325 MHz flux deficiency. The conclusion is that the RSN in Mkn 297 cannot account for the major part in the flattening of its radio spectrum. Mkn 297's star formation activity is distributed over a large number of clumps visible in Hα (see Fig. 5a) which are most likely the result of a possible merger between two late spirals, as suggested by Alloin & Duflot (1979). Hecquet, Coupinot, & Maucherat (1987) perform color photometry on 44 individual knots and find values for $B-R$ between 0.5 and 2.3. This indicates different ages of the starbursts which should lead to pronounced different spectral shapes among the knots. However, the resolution in our maps is too low to extract radio spectra of individual knots. Mkn 297's radio spectrum is dominated by extended emission which is probably a superposition of the radio spectra from the large number of knots, some of them from very recent starbursts.

6.3. *II Zw 40: Purely Thermal Emission?*

II Zw 40 has a very flat spectrum unlike the galaxies discussed previously. It is most likely dominated by thermal emission with a fraction of $f_{\mathrm{th}} \gtrsim 55\%$. The large error bars of its flux density values and the small, if any, nonthermal contribution make a determination of the nonthermal spectral index very uncertain. KWB report a very steep nonthermal spectrum with $\alpha > 0.9$. Including the 325 MHz flux density measured in this work, nonthermal emission is only consistent with fits of function I_6 (describing free-free absorption with thermal emission) which have good significance for wide a range of diameters of the thermal region (Table 6b), with H II masses required for free-free absorption being lower than in the other galaxies

(Table 7). Fitting of I_6 at small diameters of the thermal region leads to unacceptably steep values for the nonthermal spectral index. The optical diameter of the H II region in II Zw 40 (see Fig. 5*b*) is about 4″ which would require a nonthermal spectral index of $\alpha \gtrsim 1.5$; this makes a free-free absorbed nonthermal emission unlikely to be the case. In short, the spectrum of II Zw 40 is certainly dominated by thermal emission.

6.4. *General Discussion*

The four galaxies with a significant flattening in their spectra are fit well with the time-dependent injection scenarios as well as with free-free absorption (Mkn 314 has a strong flattening, but no fits were attempted as there is only an upper limit for the 325 MHz flux density). To distinguish between these interpretations, we tried to invoke results from optical color measurements. Thuan (1983) sets an upper limit to the ages of the star bursts in BCDGs from $U-B$ and $B-V$ colors to less than 5×10^7 yr. Table 8 gives in column (1) and (2) the galactic extinction–corrected $U-B$ and $B-V$ colors taken from the RC3 (de Vaucouleurs et al. 1991). Column (3) lists the optical diameter $\Theta_{\rm op}$ taken over from Table 1. Columns (4) and (5) list the FWHP diameter of the 20 cm continuum emission, and column (6), the ratio $\Theta_{\rm op}/\Theta_{1.4}$. No correlations between the radio spectral properties and colors have been found. A weak correlation between the $U-B$ colors and the ratio $\Theta_{\rm op}/\Theta_{1.4}$ exists, so that optically relatively large galaxies have redder colors. However, this is based on just six points of which two are unreliable. The relatively red $U-B$ colors of III Zw 102 suggest that its starburst has ended. No colors are available for Haro 15, but its large size $\Theta_{1.4}$ suggests that the CR electrons could have diffused over large distances since the resumption of a starburst. An estimate of the starburst history of Haro 15 based on the stellar synthesis of UV spectra (Fanelli, O'Connell, & Thuan 1988) does indicate that the *current* observed starburst is not older than about 10^7 years and an underlying A star population indicates either a sequence of short starbursts separated by a few 10^7 yr or continuous star formation throughout the last Gyr. It is more likely to observe H II galaxies at which the starburst has already ceased, than galaxies with an ongoing starburst. This has also been found in evolutionary synthesis models of star bursts (e.g., Krüger et al. 1991). The duration of the starburst itself is typically a few 10^6 yr whereas the blue colors which define H II galaxies are observable for several 10^7 yr. Synchrotron aging modifies the radio spectra in the observed frequency range in a narrow time window of a few 10^6 yr (see § 6.1). This would explain the observation of radio spectra which do not show any aging, as with II Zw 70 and Mkn 297. However, at this time we are unable to find a possible evolutionary sequence correlated with the radio spectra.

The addition of the low-frequency data to the previously known radio spectra modifies some of the conclusions drawn by KWB. The observation of the spectral flattening at low frequencies and the small size of our sample does not alter the previous observation of the overall flatness of H II galaxies' radio spectra. Among the five galaxies on which KWB perform thermal-nonthermal separations, they find four galaxies with very steep nonthermal components with spectral indices larger than $\alpha \approx 0.9$ and up to $\alpha \approx 2.1$ (see KWB's Table 7). The value established for nonthermal spiral galaxies is $\langle\alpha\rangle = 0.88$ and a thermal fraction at 1 GHz of $f_{\rm th} < 10\%$ (Gioia, Gregorini, & Klein 1982). In our work, we find a very steep nonthermal spectral index only for II Zw 70 with $\alpha = 1.2 \pm 0.4$, a galaxy where thermal and nonthermal emission can be separated easily. Our models for free-free absorption assume an underlying nonthermal emission with a straight power law. The results from these fits (fit I_6) for Haro 15, Mkn 297, and III Zw 102 are in the range $\alpha_{\rm nth} = 0.59$–0.89 for all fits with good statistical significances.

The nonthermal spectral index α makes sense only if an underlying nonthermal emission with a power-law spectrum is assumed. A more meaningful parameter, the spectral index of the *injected* electron distribution, γ_0, has been derived for all model fits and gives information about possible acceleration mechanisms of the relativistic electrons. In deriving γ_0, we assume a power law of the injected electron distribution, as is predicted by all common CR acceleration mechanisms. The results of models which predict non–power-law radio spectra across the observed frequency range, i.e., the synchrotron aging models and "different electron energy losses at different frequencies" (§ 6.2.2), can now be compared with the models which assume an underlying power-law nonthermal emission which is modified in some way (free-free absorption models and thermal-nonthermal separation). In that latter case, the derivation of γ_0 assumes that synchrotron and inverse Compton losses dominate the electrons responsible for the nonthermal emission; then $\gamma_0 = 2\ \alpha$. The fits to synchrotron aging (fits I_1 and I_2) do not assume any thermal emission and give only the injected electron spectral index γ_0, but these values do not disagree significantly with those derived from fits with free-free absorption. Including Mkn 527, the derived values for the good fits are $\gamma_0 \approx 1.1$–1.8, which does not disagree with supernova remnants as the main source of CR electrons. The spectrum of II Zw 40 is likely dominated by thermal emission with $f_{\rm th} \approx 60\%$ and might have a steep nonthermal component, but, it is not possible to set any limits on the spectral index. We do not find the nonthermal spectral indices in our sample of H II galaxies very different from normal spirals, which indicates that the relativistic electrons undergo generally the same acceleration and loss mechanisms.

Throughout this paper, several calculations depend on the magnetic field strengths derived from energy equipartition calculations. We obtain B fields up to $30 \approx \mu$G (see Table 5), and we base the results from the model fits for synchrotron aging on them. The most uncertain factor influencing the equipartition calculation is the uncertainty of the emission volume. Equipartition might also be violated by the temporal nature of the star bursts, with a relatively large number of relativistic electrons being injected over short times. The ages of the starburst derived from synchrotron aging models are of the order of one to a few 10^6 yr. Typical values for the magnetic fields of

TABLE 8

OPTICAL COLORS, OPTICAL AND CONTINUUM EMISSION SIZES

Name (1)	$U-B$ (2)	$B-V$ (3)	$\Theta_{\rm op}$ (4)	$\Theta_{1.4}$ (5)	$\Theta_{1.4}$ (kpc) (6)	$\Theta_{\rm op}/\Theta_{1.4}$ (7)
II Zw 70	−0.79	0.16	44″	<25″	<2.1	>1.8
Mkn 527	0.24	0.73	85	7.1	1.7	12
Mkn 297	−0.48	0.36	56	12.8	3.9	4.4
Mkn 314	−0.34	0.38	55	11.4	1.7	4.8
III Zw 102	0.13	0.70	95	17.5	2.1	5.4
Haro 15	...	...	51	16.5	7.6	3.1

NOTE.—The galaxies are sorted by increasing strength of the spectral break.

normal galaxies are 5–10 μG. With these magnetic field strengths the synchrotron aging models would result in more plausible ages of $\approx 10^7$ yr. With even lower magnetic fields, it cannot be excluded that CR electrons from a previous starburst contribute a significant fraction of the emission.

To improve the discrimination between the models, extensions of the known spectra to either frequency end would be needed. This could rule out some of the fits. Widening the known spectrum allows improved separations of the radio fluxes into thermal and nonthermal components. Knowing the fraction of thermal emission may constrain free-free absorption models, allow better derivations for the age of the starbursts in synchrotron aging models, and improve the estimate of the nonthermal luminosity, on which the equipartition calculations for the magnetic field strengths of these galaxies are based. Hα measurements will lead to lower limits of the emission measure and hence to lower limits of the themal emission. The case for synchrotron aging can be tested by obtaining the ratio of the luminosities $L(\mathrm{H}\alpha)/L(B)$ which gives estimates of the abundances of O stars versus A and B stars and by the determination of color coefficients, mainly $U-B$ and $B-R$. Work along these lines has been presented by Deeg (1992) and is the topic of a forthcoming paper. In conjunction with these measurements, the radio continuum spectra are a very powerful way to extract physical quantities from these remarkable galaxies as well as to date and verify their star formation history. Our analysis of the radio spectra of H II galaxies shows that there is no single dominating mechanism responsible for their shape, but that they are the result of a variety of emission, absorption, and energy loss mechanisms. This indicates that H II galaxies are a rather inhomogeneous class of galaxies.

The authors wish to thank F. Owen for suggestions improving the presentation of this paper, and F. Israel, R. Schlickeiser, M. Pohl, Heinz Andernach, & R. Price for helpful discussions and comments. H. Deeg acknowledges the award of an NRAO student assistantship which made this study possible and partial support from the NSF grant AST-902232 (N. Duric).

APPENDICES

MECHANISMS SHAPING THE RADIO SPECTRA

An overview is given of the mechanisms which are potentially shaping the radio continuum spectrum. Emission mechanisms are given in Appendix A, in Appendix B are mechanisms which shape the relativistic electron distribution, and in Appendix C are radiation absorption mechanisms. If no units are given in the formulae, the appropriates CGS units should be taken.

A. EMISSION MECHANISMS

A1. NONTHERMAL OR SYNCHROTRON EMISSION

If the energy spectrum of the relativistic electrons is given by $N(E)dE = KE^{-\gamma}dE$, where K is a constant and γ the spectral index of the electron distribution, then the synchrotron radiation emissivity is given by (Lang 1980)

$$\varepsilon_\nu \approx 0.933 \times 10^{-23} \alpha(\gamma) K B_\perp^{(\gamma+1)/2} \left(\frac{6.26 \times 10^{18}}{\nu}\right)^{(\gamma-1)/2} \text{ ergs s}^{-1}\text{ cm}^{-3}\text{ Hz}^{-1}\text{ rad}^{-2} , \quad \text{(A1)}$$

where $\alpha(\gamma)$ is a slowly varying function of order unity, ν is the frequency, and $B_\perp$ is the magnetic field's component vertical to the electrons velocity vector. Nonthermal radio emission is usually approximated with the power law

$$S_{\mathrm{nth}} \approx S_0(\nu/\nu_0)^{-\alpha} , \quad \text{(A2)}$$

where S_{nth} is the flux density and the spectral index α is given by

$$\alpha = (\gamma - 1)/2 . \quad \text{(A3)}$$

The frequency of maximum flux density, $\nu_{\max}$, emitted by monoenergetic electrons with energy E which are undergoing synchrotron losses, is given by

$$\nu_{\max} \approx 0.3\nu_c , \quad \text{(A4)}$$

with the critical frequency ν_c (Longair 1981; Lang 1980)

$$\nu_c(E) = 1.61 \times 10^{-5} B \left(\frac{E}{eV}\right)^2 \sin \vartheta , \quad \text{(A5)}$$

where ϑ is the pitch angle between the electron velocity vector and the magnetic field direction.

A2. THERMAL OR FREE-FREE EMISSION

Thermal or free-free emission is collisional bremsstrahlung emitted from *thermal* electrons in an ionized gas. The ionized gas usually coincides with optically observable H II regions. The thermal emissivity is given by (Lang 1980)

$$\varepsilon_\nu \approx 5.4 \times 10^{-39} n_\nu Z^2 \frac{n_i n_e}{T^{1/2}} g(\nu, T) \exp(-h\nu/kT) \text{ ergs s}^{-1}\text{ cm}^{-3}\text{ Hz}^{-1}\text{ rad}^{-2} . \quad \text{(A6)}$$

For the thermal radio emission from the H II region with temperature $T \approx 10^4$ K, the index of refraction is $n_\nu \approx 1$, the charge $Z \approx 1$, the electron and ion densities are $n_e \approx n_i$, $\exp(-h\nu/kT) \approx 1 - h\nu/kT \approx 1$, and the Gaunt factor, $g(\nu, T)$ can be approximated by

$$g(\nu, T) \approx 0.54 \ln [5.0 \times 10^7 (T^{3/2}/Z\nu)] . \tag{A7}$$

The frequency dependence of ε_ν depends entirely on the Gaunt factor. For $T \approx 10^4$ K and frequencies of $\nu \approx 10^9$ Hz, the Gaunt factor can be approximated by a power law with spectral index of $\alpha \approx -0.1$. This allows the common expression of the thermal emission through the power law

$$S_{\rm th} \approx S_0(\nu/\nu_0)^{-0.1} . \tag{A8}$$

It should be noted that the spectral index is temperature dependent, and for $T \approx 10^3$ K, it is approximately $S_{\rm th} \approx S_0(\nu/\nu_0)^{-0.2}$.

B. PROCESSES SHAPING THE ENERGY SPECTRUM OF THE RELATIVISTIC ELECTRONS

B1. RADIO SPECTRA FROM ELECTRONS UNDERGOING LOSSES IN THE STEADY STATE CASE

The electron energy distribution $N(E)dE$ can be obtained by solving the energy-transport equation for cosmic-ray electrons:

$$\frac{\partial N(E, t)}{\partial t} + \frac{\partial}{\partial E} [N(E, t)\varphi(E)] = q(E, t) , \tag{B1}$$

where N is the number density of electrons and $\varphi(E) = dE/dt$ is the electron energy loss rate, which depends on the particular loss mechanism. q is the source function describing the number of electrons injected per unit time and unit energy interval. In the simple case of a steady state situation, i.e., q and $N(E)$ is constant in time, the solution to equation (B1) is

$$N(E) = \varphi^{-1} \int q(e) dE . \tag{B2}$$

Using a power-law source function $q(E) = q_0 E^{-\gamma_0}$ and a loss function of the form $\varphi(E) = \xi E^\kappa$ we obtain

$$N(E) = q_0(\gamma_0 - 1)^{-1} E^{-(\gamma_0 + \kappa - 1)} . \tag{B3}$$

With the relation between the spectral indices of the electron radiation and the synchrotron emission given by equation (A3), the emitted synchrotron radiation is then given by

$$S_\nu \sim \nu^{-(\gamma_0 + \kappa - 2)/2} . \tag{B4}$$

B2. SYNCHROTRON AND COMPTON LOSSES

The synchrotron loss of a CR electron, with $B_\perp$ as the magnetic field component vertical to its path, is given by (e.g., Pacholczyk 1970):

$$-\left(\frac{\dot{E}_{\rm sync}}{\text{eV s}^{-1}}\right) = \left(\frac{E}{\rm eV}\right)^2 \times 3.80 \times 10^{-15} B_\perp^2 = E^2 \xi_{\rm syn} . \tag{B5}$$

Relativistic electrons interacting with photons of the intergalactic and interstellar radiation field undergo inverse Compton losses. The formula for the energy loss is given by (Pacholczyk 1970)

$$-\left(\frac{\dot{E}_{\rm comp}}{\text{eV s}^{-1}}\right) = \left(\frac{E}{\rm eV}\right)^2 \times 1.02 \times 10^{-25} \left(\frac{\mu_{\rm rad}}{\text{eV cm}^{-3}}\right)^2 = E^2 \xi_{\rm com} , \tag{B6}$$

where $\mu_{\rm rad}$ is the energy density of the electromagnetic radiation. For a steady state case, synchrotron and inverse Compton losses result in a steepening of the observed electron distribution $N(E) \sim E^{-\gamma}$ by a power of 1 against the injected distribution $q(E) \sim E^{-\gamma_0}$, i.e., $\gamma = \gamma_0 + 1$; see equation (B3) with $\kappa = 2$. Using equation (B4), the synchrotron radiation spectrum from electrons dominated by synchrotron *losses* is then given by

$$S(\nu) \sim \nu^{-(\gamma - 1)/2} \sim \nu^{-\gamma_0/2} . \tag{B7}$$

Two time-dependent solutions of equation (B1) for synchrotron losses are discussed by Kardashev (1962, 1964). A shortened presentation is given by Pacholczyk (1970), which has been adopted here. The first case assumes an initial distribution of electrons at a time t' ago which is not replenished any time later:

$$N(E, 0)dE = N_0 E^{-\gamma_0} . \tag{B8}$$

This is identical to a source function which represents a ne-time injection of the electrons a time t' ago:

$$q(E, t) = q_0 E^{-\gamma_0} \delta(t - t') , \tag{B9}$$

where δ is the Dirac delta function. The emitted synchrotron radiation is expressed as a function of the normalized frequency $\tilde{x}_T$ and the electron spectral index γ_0:

$$S(\nu) \sim \tilde{B}(\tilde{x}_T, \gamma_0) . \tag{B10}$$

The normalized frequency is $\tilde{x}_T = \nu/\tilde{\nu}_T$, where the break frequency $\tilde{\nu}_T$ is the critical frequency of electrons of the characteristic energy $\tilde{E}_T = (\xi_{\rm syn} t')^{-1}$. Using the frequency-energy relation given in equation (A5), with synchrotron losses only, one finds

$$\tilde{\nu}_T = 1.116 \times 10^{24} B^{-3} t'^{-2} . \tag{B11}$$

The function $\tilde{B}$ is given by

$$\tilde{B}(\tilde{x}_T, \gamma_0) = \int_0^{\pi/2} (\sin \vartheta)^{2\gamma_0} B(\tilde{x}_T \sin^3 \vartheta, \gamma_0) d\vartheta , \tag{B12}$$

where

$$B(x_T, \gamma_0) = x_T^{(1-\gamma_0)/2} \int_{x_T}^{\infty} F(z) z^{-1/2} (z^{1/2} - x_T^{1/2})^{(\gamma_0 - 2)} dz \tag{B13}$$

with

$$F(z) = z \int_z^{\infty} K_{5/3}(x) dx . \tag{B14}$$

$K_{5/3}$ is a modified Bessel function of order 5/3. $B(x_T, \gamma_0)$ is the emission from an ensemble of electrons with the same pitch angle (i.e., the angle between the velocity vector and the magnetic field is uniform) whereas $\tilde{B}(\tilde{x}_T, \gamma_0)$ is the emission from an ensemble of electrons with isotropized pitch angles. The pitch angles of relativistic electrons are taken to remain constant over time. $\tilde{B}(\tilde{x}_T, \gamma_0)$ was integrated numerically and is tabulated in Table 9. Tables for $B(x_T, \gamma_0)$ and $\tilde{B}(\tilde{x}_T, \gamma_0)$ for a smaller range of spectral indices γ are given

TABLE 9

THE FUNCTION $\tilde{B}(\tilde{x}_T, \gamma)$

	γ							
$\tilde{x}_T$	1.25	1.50	1.75	2.00	2.25	2.50	2.75	3.00
1.000e-03	7.714e+00	1.264e+01	2.366e+01	4.699e+01	9.755e+01	2.104e+02	4.604e+02	1.034e+03
1.334e-03	7.487e+00	1.179e+01	2.125e+01	4.068e+01	8.141e+01	1.693e+02	3.571e+02	7.734e+02
1.778e-03	7.306e+00	1.102e+01	1.910e+01	3.521e+01	6.788e+01	1.361e+02	2.765e+02	5.772e+02
2.371e-03	7.153e+00	1.032e+01	1.717e+01	3.046e+01	5.655e+01	1.092e+02	2.138e+02	4.300e+02
3.162e-03	7.021e+00	9.665e+00	1.544e+01	2.635e+01	4.708e+01	8.759e+01	1.651e+02	3.199e+02
4.217e-03	6.906e+00	9.062e+00	1.389e+01	2.278e+01	3.917e+01	7.017e+01	1.273e+02	2.376e+02
5.623e-03	6.838e+00	8.502e+00	1.249e+01	1.968e+01	3.256e+01	5.615e+01	9.798e+01	1.761e+02
7.499e-03	6.784e+00	7.983e+00	1.123e+01	1.699e+01	2.703e+01	4.486e+01	7.530e+01	1.303e+02
1.000e-02	6.726e+00	7.498e+00	1.010e+01	1.462e+01	2.241e+01	3.579e+01	5.774e+01	9.618e+01
1.333e-02	6.671e+00	7.045e+00	9.071e+00	1.259e+01	1.855e+01	2.849e+01	4.418e+01	7.080e+01
1.778e-02	6.621e+00	6.621e+00	8.143e+00	1.083e+01	1.533e+01	2.263e+01	3.370e+01	5.195e+01
2.371e-02	6.575e+00	6.220e+00	7.302e+00	9.305e+00	1.265e+01	1.789e+01	2.562e+01	3.797e+01
3.162e-02	6.530e+00	5.840e+00	6.513e+00	7.976e+00	1.041e+01	1.403e+01	1.940e+01	2.763e+01
4.217e-02	6.483e+00	5.477e+00	5.812e+00	6.817e+00	8.532e+00	1.100e+01	1.462e+01	2.000e+01
5.623e-02	6.428e+00	5.127e+00	5.174e+00	5.805e+00	6.963e+00	8.586e+00	1.095e+01	1.439e+01
7.499e-02	6.361e+00	4.786e+00	4.592e+00	4.920e+00	5.650e+00	6.661e+00	8.151e+00	1.027e+01
1.000e-01	6.274e+00	4.450e+00	4.055e+00	4.146e+00	4.553e+00	5.128e+00	6.015e+00	7.267e+00
1.333e-01	6.159e+00	4.115e+00	3.559e+00	3.467e+00	3.638e+00	3.912e+00	4.394e+00	5.085e+00
1.778e-01	6.004e+00	3.778e+00	3.098e+00	2.872e+00	2.876e+00	2.951e+00	3.170e+00	3.512e+00
2.371e-01	5.799e+00	3.434e+00	2.667e+00	2.351e+00	2.243e+00	2.196e+00	2.254e+00	2.388e+00
3.162e-01	5.532e+00	3.082e+00	2.265e+00	1.896e+00	1.712e+00	1.605e+00	1.573e+00	1.592e+00
4.217e-01	5.191e+00	2.719e+00	1.889e+00	1.500e+00	1.285e+00	1.150e+00	1.074e+00	1.037e+00
5.623e-01	4.767e+00	2.347e+00	1.541e+00	1.159e+00	9.420e-01	8.019e-01	7.134e-01	6.566e-01
7.499e-01	4.258e+00	1.970e+00	1.221e+00	8.691e-01	6.699e-01	5.420e-01	4.587e-01	4.019e-01
1.000e+00	3.671e+00	1.597e+00	9.338e-01	6.288e-01	4.591e-01	3.528e-01	2.837e-01	2.364e-01
1.334e+00	3.030e+00	1.240e+00	6.842e-01	4.358e-01	3.013e-01	2.197e-01	1.677e-01	1.329e-01
1.778e+00	2.376e+00	9.158e-01	4.772e-01	2.875e-01	1.884e-01	1.303e-01	9.442e-02	7.104e-02
2.371e+00	1.760e+00	6.406e-01	3.158e-01	1.802e-01	1.120e-01	7.349e-02	5.059e-02	3.617e-02
3.162e+00	1.234e+00	4.257e-01	1.991e-01	1.079e-01	6.369e-02	3.974e-02	2.601e-02	1.769e-02
4.217e+00	8.306e-01	2.728e-01	1.215e-01	6.269e-02	3.524e-02	2.094e-02	1.306e-02	8.458e-03
5.623e+00	5.505e-01	1.727e-01	7.344e-02	3.618e-02	1.941e-02	1.100e-02	6.544e-03	4.042e-03
7.499e+00	3.683e-01	1.105e-01	4.491e-02	2.113e-02	1.083e-02	5.858e-03	3.325e-03	1.959e-03
1.000e+01	2.510e-01	7.198e-02	2.794e-02	1.256e-02	6.140e-03	3.170e-03	1.716e-03	9.648e-04
1.334e+01	1.736e-01	4.754e-02	1.761e-02	7.553e-03	3.523e-03	1.735e-03	8.959e-04	4.802e-04
1.778e+01	1.212e-01	3.167e-02	1.120e-02	4.579e-03	2.037e-03	9.565e-04	4.709e-04	2.407e-04
2.371e+01	8.512e-02	2.121e-02	7.152e-03	2.789e-03	1.183e-03	5.297e-04	2.487e-04	1.211e-04
3.162e+01	5.999e-02	1.426e-02	4.585e-03	1.705e-03	6.897e-04	2.944e-04	1.317e-04	6.118e-05

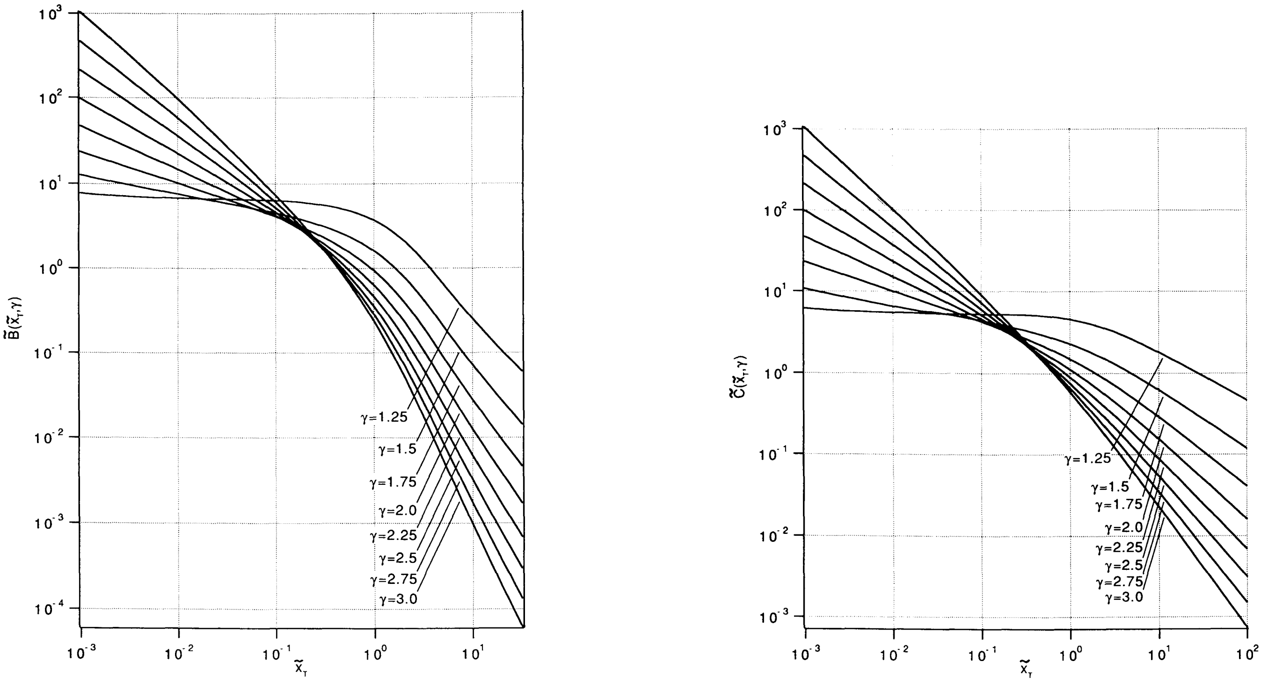

FIG. 6*a* FIG. 6*b*

FIG. 6.—(*a*) Plot of the function $\tilde{B}(\tilde{x}_T, \gamma)$. (*b*) Plot of the function $\tilde{C}(\tilde{x}_T, \gamma)$

by Pacholczyk (1977) as well. Graphs of $\tilde{B}(\tilde{x}_T, \gamma_0)$ for various values of γ are presented in Figure 6*a*. Approximations for the low- and high-frequency regions are from Pacholczyk (1977):

$$S(\nu) \sim \nu^{-(\gamma_0 - 1)/2}\,, \qquad \nu \ll \tilde{\nu}_T \tag{B15}$$

and

$$S(\nu) - \nu^{-(2\gamma_0 + 1)/3}\,, \qquad \tilde{\nu} \gg \nu_T\,. \tag{B16}$$

The break in the spectral index is then given by

$$\Delta\alpha = (\gamma_0 + 5)/6 \tag{B17}$$

The second time-dependent case considers the injection of CR electrons which began a time t' ago:

$$q(E, t) = \begin{cases} q_0 E^{-\gamma_0}\,; & t > t' \\ 0 \;\;\;\;\;\;\; ; & t < t'\,. \end{cases} \tag{B18}$$

The resulting spectra are given by

$$S(\nu) \sim \tilde{C}(\tilde{x}_T, \gamma_0) \tag{B19}$$

where $\tilde{x}_T$ is the normalized frequency as before and

$$\tilde{C}(\tilde{x}_T, \gamma_0) = \int_0^{\pi/2} (\sin \vartheta)^{2\gamma_0} C(\tilde{x}_T \sin^3 \vartheta, \gamma_0) d\vartheta \tag{B20}$$

with

$$C(x_T, \gamma_0) = x_T^{-\gamma_0/2} \frac{1}{\gamma - 1} \times \left[\int_0^\infty F(z) z^{(\gamma_0 - 2)/2} dz - \int_{x_T}^\infty F(z) z^{-1/2} (z^{1/2} - x_T^{1/2})^{(\gamma_0 - 1)} dz \right], \tag{B21}$$

$F(z)$ is given in equation (B14). We would like to note that equation (B21) does contain an error in the first term in Pacholczyk (1970). Graphs of $\tilde{C}(\tilde{x}_T, \gamma_0)$ are shown in Figure 6*b* and tabulated in Table 10. Approximations for the low- and high-frequency regions are

$$S(\nu) \sim \nu^{-(\gamma_0 - 1)/2}\,, \qquad \nu \ll \tilde{\nu}_T \tag{B22}$$

and

$$S(\nu) \sim \nu^{-\gamma_0/2}\,, \qquad \nu \gg \tilde{\nu}_T\,, \tag{B23}$$

TABLE 10

THE FUNCTION $\tilde{C}(\tilde{x}_T, \gamma)$

	γ							
$\tilde{x}_T$	1.25	1.50	1.75	2.00	2.25	2.50	2.75	3.00
1.000e-03	6.149e+00	1.069e+01	2.292e+01	4.682e+01	9.841e+01	2.122e+02	4.684e+02	1.056e+03
1.334e-03	5.981e+00	9.986e+00	2.060e+01	4.056e+01	8.218e+01	1.709e+02	3.638e+02	7.907e+02
1.778e-03	5.855e+00	9.352e+00	1.854e+01	3.514e+01	6.862e+01	1.375e+02	2.822e+02	5.915e+02
2.371e-03	5.753e+00	8.774e+00	1.669e+01	3.045e+01	5.727e+01	1.106e+02	2.188e+02	4.422e+02
3.162e-03	5.668e+00	8.242e+00	1.503e+01	2.639e+01	4.779e+01	8.893e+01	1.696e+02	3.303e+02
4.217e-03	5.598e+00	7.752e+00	1.355e+01	2.286e+01	3.986e+01	7.146e+01	1.313e+02	2.465e+02
5.623e-03	5.542e+00	7.299e+00	1.221e+01	1.981e+01	3.324e+01	5.739e+01	1.016e+02	1.839e+02
7.499e-03	5.497e+00	6.880e+00	1.100e+01	1.716e+01	2.770e+01	4.605e+01	7.854e+01	1.370e+02
1.000e-02	5.463e+00	6.493e+00	9.919e+00	1.485e+01	2.307e+01	3.693e+01	6.067e+01	1.019e+02
1.333e-02	5.439e+00	6.133e+00	8.941e+00	1.285e+01	1.920e+01	2.958e+01	4.680e+01	7.577e+01
1.778e-02	5.378e+00	5.800e+00	8.057e+00	1.111e+01	1.596e+01	2.367e+01	3.606e+01	5.624e+01
2.371e-02	5.316e+00	5.580e+00	7.258e+00	9.605e+00	1.326e+01	1.892e+01	2.774e+01	4.167e+01
3.162e-02	5.271e+00	5.420e+00	6.534e+00	8.291e+00	1.100e+01	1.509e+01	2.131e+01	3.081e+01
4.217e-02	5.245e+00	5.161e+00	5.878e+00	7.148e+00	9.106e+00	1.202e+01	1.633e+01	2.273e+01
5.623e-02	5.230e+00	4.890e+00	5.281e+00	6.153e+00	7.527e+00	9.551e+00	1.248e+01	1.673e+01
7.499e-02	5.222e+00	4.617e+00	4.738e+00	5.287e+00	6.208e+00	7.571e+00	9.518e+00	1.227e+01
1.000e-01	5.218e+00	4.345e+00	4.242e+00	4.532e+00	5.106e+00	5.983e+00	7.233e+00	8.983e+00
1.333e-01	5.212e+00	4.077e+00	3.790e+00	3.874e+00	4.187e+00	4.712e+00	5.475e+00	6.542e+00
1.778e-01	5.196e+00	3.816e+00	3.375e+00	3.300e+00	3.420e+00	3.696e+00	4.126e+00	4.739e+00
2.371e-01	5.164e+00	3.556e+00	2.995e+00	2.800e+00	2.781e+00	2.884e+00	3.095e+00	3.414e+00
3.162e-01	5.146e+00	3.301e+00	2.645e+00	2.364e+00	2.250e+00	2.238e+00	2.306e+00	2.443e+00
4.217e-01	5.062e+00	3.046e+00	2.323e+00	1.984e+00	1.808e+00	1.725e+00	1.706e+00	1.735e+00
5.623e-01	4.931e+00	2.791e+00	2.026e+00	1.652e+00	1.442e+00	1.319e+00	1.252e+00	1.223e+00
7.499e-01	4.754e+00	2.535e+00	1.751e+00	1.365e+00	1.140e+00	1.000e+00	9.103e-01	8.535e-01
1.000e+00	4.527e+00	2.279e+00	1.499e+00	1.116e+00	8.924e-01	7.504e-01	6.554e-01	5.901e-01
1.334e+00	4.251e+00	2.024e+00	1.268e+00	9.023e-01	6.911e-01	5.572e-01	4.670e-01	4.038e-01
1.778e+00	3.927e+00	1.773e+00	1.060e+00	7.210e-01	5.291e-01	4.092e-01	3.293e-01	2.735e-01
2.371e+00	3.568e+00	1.530e+00	8.738e-01	5.692e-01	4.005e-01	2.973e-01	2.299e-01	1.835e-01
3.162e+00	3.188e+00	1.303e+00	7.116e-01	4.444e-01	3.001e-01	2.140e-01	1.590e-01	1.221e-01
4.217e+00	2.805e+00	1.095e+00	5.732e-01	3.435e-01	2.229e-01	1.528e-01	1.092e-01	8.073e-02
5.623e+00	2.438e+00	9.113e-01	4.577e-01	2.636e-01	1.644e-01	1.085e-01	7.463e-02	5.311e-02
7.499e+00	2.099e+00	7.526e-01	3.632e-01	2.011e-01	1.207e-01	7.666e-02	5.079e-02	3.481e-02
1.000e+01	1.796e+00	6.183e-01	2.869e-01	1.528e-01	8.832e-02	5.401e-02	3.447e-02	2.277e-02
1.334e+01	1.530e+00	5.060e-01	2.259e-01	1.158e-01	6.446e-02	3.797e-02	2.335e-02	1.486e-02
1.778e+01	1.298e+00	4.129e-01	1.774e-01	8.759e-02	4.695e-02	2.665e-02	1.580e-02	9.691e-03
2.371e+01	1.099e+00	3.362e-01	1.391e-01	6.613e-02	3.416e-02	1.868e-02	1.068e-02	6.313e-03
3.162e+01	9.278e-01	2.732e-01	1.088e-01	4.986e-02	2.482e-02	1.309e-02	7.207e-03	4.109e-03
4.217e+01	7.821e-01	2.217e-01	8.507e-02	3.756e-02	1.802e-02	9.158e-03	4.863e-03	2.674e-03
5.623e+01	6.583e-01	1.797e-01	6.643e-02	2.827e-02	1.307e-02	6.406e-03	3.280e-03	1.739e-03
7.499e+01	5.535e-01	1.455e-01	5.184e-02	2.126e-02	9.478e-03	4.478e-03	2.211e-03	1.130e-03
1.000e+02	4.649e-01	1.178e-01	4.042e-02	1.598e-02	6.869e-03	3.130e-03	1.490e-03	7.348e-04

i.e., $S(\nu)$ changes its spectral index by $\frac{1}{2}$ across the frequency range. The time-dependent solutions discussed so far are valid for ensembles of electrons for which the pitch angles are preserved. If the pitch angles gets constantly isotropized, or if the energy losses are dominated by inverse Compton losses, then the enerrgy losses are independent of the *initial* pitch angles. This will modify the case of an initial electron distribution which is not replenished since time t' ago. Now the spectrum has a high-energy cutoff at energy $\tilde{E}_T = (\xi t')^{-1}$ where $\xi = \xi_{\text{syn}} + \xi_{\text{com}}$. This results in very steep spectra for $\nu > \tilde{\nu}_T$, as is discussed in the main paper for injection spectra with high-energy cutoffs. The break frequency $\tilde{\nu}_T$ for combined synchrotron and inverse Compton losses is given by

$$\tilde{\nu}_T = \frac{B}{t^2[9.47 \times 10^{-13} B^2 + 2.54 \times 10^{-23}(\mu_{\text{rad}}/\text{eV cm}^{-3})]^2} . \tag{B24}$$

If losses independent of the pitch angle dominate in the case of a continuous electron injection beginning a time t' ago, the spectral break of $\Delta\alpha = 0.5$ will occur over a narrower frequency regime compared to equation (B20) or to Figure 6*b*, but the break frequency is again given by equation (B24).

B3. ELECTRON ENERGY LOSSES BY INELASTIC FREE-FREE ENCOUNTERS (RELATIVISTIC BREMSSTRAHLUNG)

Relativistic electrons lose energy by free-free encounters with neutral hydrogen (H I) of number density $n_{\mathrm{H\,I}}$ at a rate of Pacholczyk 1970)

$$-\frac{\dot{E}_{\mathrm{ff}}}{E} = 7.26 \times 10^{-16} n_{\mathrm{H\,I}} \tag{B25}$$

In fully ionized hydrogen (H II) of density $n_{\mathrm{H\,II}}$ the loss rate is

$$-\frac{\dot{E}_{\mathrm{ff}}}{E} = 1.37 \times 10^{-16} n_{\mathrm{H\,II}} \left[\ln\left(\frac{E}{\mathrm{eV}}\right) - 12.78 \right] = \eta_{\mathrm{ff}} \,. \tag{B26}$$

Free-free losses of relativistic electrons do not change the spectral index of a distribution of electrons. For electron energies of 10^8–10^{10} eV the loss rates from free-free losses in H I and H II are of the same order of magnitude if the number densities of H I and H II are about the same.

B4. CONVECTIVE ELECTRON ENERGY LOSSES

The electron energy loss by adiabatic deceleration in a dynamical halo is given by (Lerche & Schlickeiser 1982)

$$-\frac{\dot{E}_{\mathrm{conv}}}{E} = \frac{1}{3}(\nabla\bar{v}) = \eta_{\mathrm{conv}} \,, \tag{B27}$$

where $\bar{v}$ is the wind velocity out of the galaxy. For a spherical geometry with constant wind velocity is $\nabla\bar{v} = v/R$. The work by Lerche & Schlickeiser (1982) and Pohl & Schlickeiser (1990) shows that the integrated radio emission of a galaxy with adiabatic deceleration losses has a spectral break of $\Delta\alpha = 0.5$ from low frequencies, where adiabatic deceleration losses dominate, toward higher frequencies, where synchrotron and inverse Compton losses dominate.

B5. COULOMB AND IONIZATION LOSSES

Coulomb losses are elastic two-body scatterings between electrons and a medium; they dominate at lower electron energies when bremsstrahlung radiation becomes insignificant. In fully ionized H II of density $n_{\mathrm{H\,II}}$ they are (Pacholczyk 1970; Gould 1975)

$$-\left(\frac{\dot{E}_{\mathrm{ion}}}{\mathrm{eV\ s^{-1}}}\right) = 7.62 \times 10^{-9} n_{\mathrm{H\,II}} \left[\ln\left(\frac{E}{\mathrm{eV}}\right) + 60.3 - \ln\left(\frac{n_{\mathrm{H\,II}}}{\mathrm{cm^{-3}}}\right) \right] . \tag{B28}$$

In neutral media, the electrons undergo additional losses through ionization of the medium. Frequently, both Coulomb and ionization losses are just referred to as "ionization losses." The combined ionization and Coulomb losses are given for H I as

$$-\left(\frac{\dot{E}_{\mathrm{ion}}}{\mathrm{eV\ s^{-1}}}\right) = 2.29 \times 10^{-8} n_{\mathrm{H\,II}} \left[\ln\left(\frac{E}{\mathrm{eV}}\right) - 6.87 \right] , \tag{B29}$$

where $n_{\mathrm{H\,I}}$ is the density of atomic hydrogen. Coulomb and ionization losses of relativistic electrons lead to a flattening of an electron distribution $N(E)$ from $N(E) \alpha E^{-\gamma_0}$ to $N(E) \alpha E^{-(\gamma_0 - 1)}$. The near independence of the loss rate from the electron energy renders these losses more significant at lower energies. However, using $n = 10\ \mathrm{cm^{-3}}$ it follows from equation (B29) that ionization losses are insignificant at electron energies which correspond to radio frequencies of more than 50 MHz.

C. RADIATION ABSORPTION MECHANISMS

C1. RAZIN-TSYTOVICH EFFECT OR PLASMA EFFECT

Synchrotron absorption at low frequencies due to thermal electrons in the source causes a departure from unity of the refractive index of the medium. This effect becomes significant at frequencies below ν_s:

$$\nu_s \approx 20 n_e B^{-1} \,. \tag{C1}$$

Here n_e is the number density of thermal electrons and B the magnetic field strength.

C2. SYNCHROTRON SELF-ABSORPTION

Synchrotron self-absorption is of significance only in sources with a very high radio surface brightness and is insignificant in the observed H II galaxies as can be shown by calculating the critical frequency ν_{ss} below which self-absorption becomes significant. For a source with negligible redshift, ν_{ss} is given by (Lang 1980)

$$\left(\frac{\nu_{\mathrm{ss}}}{\mathrm{MHz}}\right) \approx 34 \left(\frac{S_{\nu_{\mathrm{ss}}}}{\mathrm{Jy}}\right)^{2/5} \left(\frac{\theta}{\mathrm{arcsec}}\right)^{-4/5} \left(\frac{B}{\mathrm{G}}\right)^{1/5} . \tag{C2}$$

$S_{\nu_{\mathrm{ss}}}$ is the flux density at frequency ν_{ss}, ν_{ss}, θ is the angular size of the source, and B is the magnetic field. $S_{\nu_{\mathrm{ss}}}$ is not known a priori, but if the flux density depends as a power law with a spectral index α on the frequency, it is $S_{\nu_{\mathrm{ss}}} = S_\nu(\nu_{\mathrm{ss}}/\nu)^{-\alpha}$, where S_ν is a flux density measured at a frequency $\nu > \nu_{\mathrm{ss}}$. The critical frequency can then be obtained by

$$\left(\frac{\nu_{\mathrm{ss}}}{\mathrm{MHz}}\right) \approx \left[4.5 \times 10^7 \left(\frac{S_\nu}{\mathrm{Jy}}\right)^2 \left(\frac{\nu}{\mathrm{MHz}}\right)^{2\alpha} \left(\frac{\theta}{\mathrm{arcsec}}\right)^{-4} \left(\frac{B}{\mathrm{G}}\right) \right]^{1/(5+2\alpha)} . \tag{C3}$$

The spectral index for a synchrotron self absorbed source is $\alpha = 2.5$ for $\nu < \nu_{\mathrm{ss}}$.

C3. FREE-FREE ABSORPTION OF BREMSSTRAHLUNG SELF-ABSORPTION

Electromagnetic radiation gets free-free absorbed in an ionized gas by thermal electrons interacting with protons. The optical depth at a frequency ν, emission measure EM, and electron temperature T_e is given by (Mezger & Henderson 1967; Altenhoff et al. 1960)

$$\tau_\nu = 8.3 \times 10^{-2} T_e^{-1.35} \left(\frac{EM}{\mathrm{pc\ cm^{-6}}}\right) \left(\frac{\nu}{\mathrm{GHz}}\right)^{-2.1} \tag{C4}$$

with $\mathrm{EM} = \int n_{\mathrm{H\,II}}^2 dl$, $n_{\mathrm{H\,II}}$ is the H II density The way free-free absorption shapes a radio spectrum depends on the geometry of the emission and absorption region:

If an absorbing region of optical depth τ is positioned between the emission region and the observer, the observed flux density S is $S = S_0 \exp(-\tau)$, where S_0 is the flux density of the emission region. With $S_0 \sim \nu^{-\alpha}$ the observed spectrum will be given by

$$S_\nu \sim \nu^{-\alpha} \exp(-\tau_\nu) . \tag{C5}$$

If the emission and absorption are in the same volume, the observed radiation is

$$S_\nu = \varepsilon_\nu / \kappa_\nu [1 - \exp(-\tau_\nu)] , \tag{C6}$$

where ε_ν is the emission coefficient. In the case of synchrotron radiation ε_ν will be a power law, $\varepsilon_\nu \sim \nu^{-\alpha}$. κ_ν is the absorption coefficient, which depends like equation (C4) on the frequency as $\kappa_\nu \sim \nu^{-2.1}$. This leads to S_ν being dependent on the frequency as

$$S_\nu \sim \nu^{-\alpha+2.1} [1 - \exp(-\tau_\nu)] . \tag{C7}$$

REFERENCES

Alloin, D., & Duflot, R. 1979, A&A, 78, L5

Altenhoff, W., Mezger, P. G., Strassl, H., Wendker, H., & Westerhout, G. 1960, Veröff. Sternwarte Bonn, 59, 48

Barrs, J. W. M., Genzel, R., Pauliny-Toth, I. I. K., & Witzel, A. 1977, A&A, 61, 99

Baldwin, J. A., Spinrad, H., & Terlevich, R. 1982, MNRAS, 198, 535

Balkowski, C., Chamaraux, P., & Weliachew, L. 1978, A&A, 69, 263

Barbieri, C., Bonoli, C., & Rafanelli, P. 1979, A&AS, 37, 541

Biermann, P., Clarke, J. N., Fricke, K. J., Pauliny-Toth, I. I. K., Schmidt, J., & Witzel, A. 1980, A&A, 81, 235

Brinks, E. 1991, NRAO Newsletter, No. 49, 4

Brinks, E., & Klein, U. 1986, in Star-Forming Dwarf Galaxies and Related Objects, ed. D. Kunth, T. X. Thuan, & J. Tran Thanh Van (Paris: Editions Frontières), 281

Chevalier, R. A. 1984, Ann. NY Acad. Sci., 422, 215

Day, G. A., Shimmins, A. J., Ekers, R. D., & Cole D. J. 1966, Australian J. Phys., 19, 35

Deeg, H. J. 1992, in Proc. of the Third Teton Summer School, The Evolution of Galaxies and Their Environment, ed. H. A. Thronson, in press

de Vaucouleurs, G., de Vaucouleurs, A., Corwin, H. G., Buta, R. J., Paturel, G., & Fouqué, P. 1991, Third Reference Catalog of Bright Galaxies (New York: Springer-Verlag) (RC3)

Dixon, R. S. 1970, ApJS, 20, 1

Dressel, L. L., & Condon, J. J. 1978, ApJS, 36, 53

Duric, N., Bourneuf, E., & Gregory, P. C. 1988, AJ, 96, 81

Fanelli, M. N., O'Connell, R. W., & Thuan, T. X. 1988, ApJ, 334, 665

Gioia, I. M., Gregorini, L., & Klein, U. 1982, A&A, 115, 164

Gould, R. J. 1975, ApJ, 196, 689

Hecquet, J., Coupinot, G., & Maucherat, A. J. 1987, ApJ, 183, 13

Heeschen, D. S., Heidmann, J., & Yin, Q. F. 1983, ApJ, 267, L73

Heidmann, J., Klein, U., & Wielebinski, R. 1982, A&A, 105, 188

Helou, G., Soifer, B. T., & Rowan-Robinson, M. 1985, ApJ, 298, L7

Högbom, J. A. 1974, A&AS, 15, 417

Hummel, E. 1991, A&A, 251, 442

Israel, F. P., & de Bruyn, A. G. 1988, A&A, 198, 109

Israel, F. P., & Mahoney, M. J. 1990, ApJ, 352, 30

Israel, F. P., Mahoney, M. J., & Howarth, N. 1992, A&A, submitted

Jaffe, W. J., Perola, G. C., & Tarenghi, M. 1978, ApJ, 224, 808

Kardashev, N. S. 1962, Soviet Astron.–AJ, 6, 317

———. 1964, Soviet Astron.–AJ, 7, 740

Klein, U., Heidmann, J., Wielebinski, R., & Wunderlich, E. 1986, A&A, 154, 373

Klein, U., Weiland, H., & Brinks, E. 1991, A&A, 246, 323 (KWB)

Klein, U., Wielebinski, R., & Beck, R. 1984a, A&A, 133, 19

Klein, U., Wielebinski, R., & Thuan, T. X. 1984b, A&A, 141, 241

Krüger, H., Fritze–von Alvensleben, U., Loose, H.-H., & Fricke, K. J. 1991, A&A, 242, 343

Lang, K. R. 1980, Astrophysical Formulae (Berlin: Springer-Verlag)

Lerche, I., & Schlickeiser, R. 1982, A&A, 107, 148

Longair, M. S. 1981, High Energy Astrophysics (Cambridge: Cambridge Univ. Press)

Lonsdale, C. J., Lonsdale, C. J., & Smith, H. E. 1992, ApJ, 391, 629

Maehara, H., Inoue, M., Takase, B., & Noguchi, T. 1985, PASJ, 37, 451

Mezger, P. G., & Henderson, A. P. 1967, ApJ, 147, 471

Pacholczyk, A. G. 1970, Radio Astrophysics (San Francisco: W. H. Freeman)

———. 1977, Radio Galaxies (Oxford: Pergamon Press)

Perley, R. A., & Cornwell, T. J. 1991, in Radio Interferometry: Theory, Techniques, and Applications, ed. T. J. Cornwell & R. A. Perley (ASP Conf. Ser., 19), 184

Pohl, M., & Schlickeiser, R. 1990, A&A, 234, 147

———. 1991, A&A, 252, 565

Pohl, M., Schlickeiser, R., & Hummel, E. 1991, A&A, 250, 302

Press, W. H., Flannery, B. P., Teukolsky, S. A., & Vetterling, W. T. 1988, Numerical Recipes in C (Cambridge: Cambridge Univ. Press)

Sargent, W. L. W., & Searle, L. 1970, ApJ, 162, L155

Skillman, E. D., & Klein, U. 1988, A&A, 199, 61

Sramek, R. A., & Weedman, D. W. 1986, ApJ, 302, 640

Sutton, J. M., Davies, I. M., Little, A. G., & Murdoch, H. S. 1974, Australian J. Phys., Astrophys. Suppl., No. 33, 1

Thuan, T. X. 1983, ApJ, 268, 667

Webber, W. R. 1991, in The Interpretation of Modern Synthesis Observation of Spiral Galaxies, ed. N. Duric & P. C. Crane (ASP Conf. Ser., 18), 37

Wunderlich, E., Klein, U., & Wielebinski, R. 1987, A&AS, 69, 487

Wynn-Williams, C. G., & Becklin, E. E. 1986, ApJ, 308, 620

Yin, Q. F., & Heeschen, D. S. 1991, Nature 354, 130